ward in the striatum reflected the nonlinearity parameter as estimated behaviorally.

A deeper question is how modulatory neurotransmission is involved in the central process of decision-making (Trepel et al., 2005; Rangel et al., 2008; Fox and Poldrack, 2009). Investigation of the relationship between the dopamine (DA) system and prospect theory seems promising, considering the fact that DA is linked to risk-seeking behavior (Leyton et al., 2002) and is involved in disrupted decision-making observed in neuropsychiatric disorders such as drug/gambling addiction and Parkinson's disease (Zack and Poulos, 2004; Steeves et al., 2009). Trepel et al. (2005) speculated in a thoughtful review that DA transmission in the striatum might be involved in shaping probability weighting. Using positron emission tomography (PET), we tested this speculation directly by investigating how DA D_1 and D_2 receptors in the brain are associated with transformation of probabilities into decision weights. Phasic DA release occurs during reward and reward-predicting stimuli (Grace, 1991; Schultz, 2007). It is suggested that available striatal D_1 receptors are preferentially stimulated by phasically released DA, whereas low-level baseline tonic DA release is enough for stimulating striatal D_2 receptors (Frank et al., 2007; Schultz, 2007). Because estimating reward cue in our task is considered to induce phasic DA release, we hypothesized that the variability of available D_1 receptors might be more associated with individual differences than that of available D_2 receptors.

Materials and Methods

Subjects

Thirty-six healthy male volunteers (mean age ± SD, 25.2 ± 4.9 years) were studied. They did not meet the criteria for any psychiatric disorder based on unstructured psychiatric screening interviews. None of the controls were taking alcohol at the time, nor did they have a history of psychiatric disorder, significant physical illness, head injury, neurological disorder, or alcohol or drug dependence. Ten subjects were light to moderate cigarette smokers. All subjects were right-handed according to the Edinburgh Handedness Inventory. The vast majority of subjects were university students or graduate school students (three of the participants had finished university and were employed). All subjects underwent MRI to rule out cerebral anatomic abnormalities. After complete explanation of the study, written informed consent was obtained from all subjects, and the study was approved by the Ethics and Radiation Safety Committee of the National Institute of Radiological Sciences, Chiba, Japan.

Procedure

To estimate decision weight, certainty equivalents were determined outside the PET scanner. The behavioral experiment took place 1–2 h before the first PET scans. The procedure was based on the staircase procedure suggested by Tversky and Kahneman (1992), which is the most efficient method for estimating certainty equivalents (Paulus and Frank, 2006; Fox and Poldrack, 2009). A gamble's certainty equivalent is the amount of sure payoff at which a player is indifferent between the sure payoff and the gamble. Participants were presented with options between a gamble and a sure payoff on a computer monitor (supplemental Fig. 1, available at www.jneurosci.org as supplemental material). Gambles were presented that had an objective probability p of paying a known outcome x (and paying zero otherwise). The different combinations of p and x are shown in supplemental Table 1, available at www.jneurosci.org as supplemental material. There were 22 gambles, and half of them were 10,000 yen (~$100) gambles. Because 10,000 yen is the highest-value Japanese paper currency, 11 probabilities were used for 10,000 yen gambles to refine the estimation of weighting function. In each trial, the participants chose between a gamble and a sure payoff. The relative position (left and right) of the two options was randomized to counterbalance for order effects. The subjects were told to make hypothetical rather than actual gambles and were instructed as follows: "Two options for possible monetary gain will be presented to you. Option 1 is a sure payoff and option 2 is a gamble. For example, you will see the guaranteed 6,666 yen on one side of the monitor, and see a gamble in which you have a 50% chance of winning 10,000 yen on the other side. Make a choice between the two options according to your preference by pressing the right or left button. There is no correct answer and no time limit. Once you make a choice, the next options will be presented."

Each time a choice was made between a gamble and a sure payoff in a trial, the amount of a sure payoff in the next trial was adjusted and eight trials per each gamble were iterated to successively narrow the range including the certainty equivalents. The adjustments in the amount of a sure payoff were made in the following manner. The initial range was set between 0 and x (the gamble outcome). The range was divided into thirds. The one-third and the two-thirds intersecting points of the initial range were used as sure payoff options in trials 1 and 2. If the participant accepted the sure option of the two-thirds and rejected that of the one-third in trials 1 and 2, the middle third portion of the initial range was used as a range for trials 3 and 4. If the participant accepted both sure options of the thirds, the lower third part was then used as a range. If the participant rejected both the sure options of the thirds, the upper third part was then used. The new range was again divided into thirds and the same procedure was iterated until the participant completed trial 8. The mean of the final range was used for a certainty equivalent (supplemental Fig. 2, available at www.jneurosci.org as supplemental material). Once a certainty equivalent was estimated for a given gamble, the next gamble was chosen for estimation, and so on. The order of the gambles was randomized across the participants.

Behavioral data estimation

According to the prospect theory, the valuation V of a prospect that pays amount x with probability p is expressed as $v(x, p) = w(p)\, v(x)$, where v is the subjective value of the amount x, and w is the decision weight of the objective probability p. The utility function is usually assumed to be a power function $v(x) = x^{\sigma}$ (results are typically similar to other functions). Although several estimations of the nonlinear probability weighing function have been used in previous experiments (Lattimore et al., 1992; Tversky and Kahneman, 1992; Wu and Gonzalez, 1996), we estimated probability weighting using the one-parameter function derived axiomatically by Prelec (1998), $w(p) = \exp\{-(\ln(1/p))^{\alpha}\}$ with $0 < \alpha < 1$. This function typically fits as well as other functions with one or two parameters (Hsu et al., 2009), and because nonlinearity is fully captured by a single parameter, it is simple to correlate the degree of nonlinearity (α) across individuals with biological measures such as receptor density or fMRI signals (Hsu et al., 2009). This $w(p)$ function has an inverted-S shape with a fixed inflection point at $p = 1/e = 0.37$ (at that point the probability $1/e$ also receives decision weight $1/e$). The parameter α indicates the degree of nonlinearity. A smaller value of α (closer to 0) means a more nonlinear inflected weighting function and a higher value (closer to 1) means a more linear weighting function. At $\alpha = 1$ the function is linear. The weighting function and utility function were estimated by least-squares method.

PET scanning

PET studies were performed on ECAT EXACT HR+ (CTI-Siemens). The system provides 63 planes and a 15.5 cm field of view. To minimize head movement, a head fixation device (Fixster) was used. A transmission scan for attenuation correction was performed using a germanium 68–gallium 68 source. Acquisitions were done in three-dimensional mode with the interplane septa retracted. The first group of 18 subjects (mean age ± SD, 24.7 ± 3.8 years) was studied for both D_1 receptors and extrastriatal D_2 receptors. These 18 subjects came to the PET center twice, once each for the studies of [^{11}C]SCH23390 (*R*-(+)-7-chloro-8-hydroxy-3-methyl-1-phenyl-2,3,4,5-tetrahydro-1*H*-3-benzazepine) and [^{11}C]FLB457 ((*S*)-*N*-((1-ethyl-2-pyrrolidinyl)methyl)-5-bromo-2,3-dimethoxybenzamide). For evaluation of D_1 receptors, a bolus of 215.9 ± 9.8 MBq of [^{11}C]SCH23390 with specific radioactivities (90.1 ± 38.5 GBq/μmol) was injected intravenously from the antecubital vein with a 20 ml saline flush. The fact that [^{11}C]SCH23390 has high affinity for D_1 receptors (Ekelund et al., 2007), and that D_1 receptors are mod-

erately expressed in the extrastriatal regions (approximately one-fifth of striatal D_1 receptor density) (Ito et al., 2008) leads to good reproducibility of both striatal and extrastriatal [^{11}C]SCH23390 bindings (Hirvonen et al., 2001). Although [^{11}C]SCH23390 is a selective radioligand for D_1 receptors, it has some affinity for $5HT_{2A}$ receptors. However, $5HT_{2A}$ receptor density in the striatum is negligible compared with D_1 receptor density. $5HT_{2A}$ receptor density is never negligible in the extrastriatal regions. Although previous reports in the literature have indicated that [^{11}C]SCH23390 affinity for $5HT_{2A}$ receptors relative to D_1 receptors is negligible, a recent *in vivo* study reported that approximately one-fourth of the cortical signal of [^{11}C]SCH23390 was due to binding to $5HT_{2A}$ receptors, suggesting that cautious interpretation of the extrastriatal findings regarding this ligand is recommended (Ekelund et al., 2007). For evaluation of extrastriatal D_2 receptors, a bolus of 218.3 ± 13.9 MBq of [^{11}C]FLB457 with high specific radioactivities (238.0 ± 100.8 GBq/μmol) was injected in the same way. [^{11}C]FLB457 has very high affinity for D_2 receptors. It is a selective radioligand for D_2 receptors and has good reproducibility of extrastriatal D_2 bindings (Sudo et al., 2001). Dynamic scans were performed for 60 min for [^{11}C]SCH23390 and 90 min for [^{11}C]FLB457 immediately after the injection. Although [^{11}C]FLB457 accumulates to a high degree in the striatum, striatal data were not evaluated since the duration of the [^{11}C]FLB457 PET study was not sufficient to obtain equilibrium in the striatum (Olsson et al., 1999; Suhara et al., 1999). For radiation safety reason, striatal D_2 receptors were evaluated in the second group of the other 18 subjects [mean age ± SD, 25.7 ± SD 5.9 years]. A bolus of 218.2 ± 10.1MBq of [^{11}C]raclopride with a specific radioactivity of 451.1 ± 154.6 GBq/μmol was injected similarly. [^{11}C]Raclopride is a selective radioligand for D_2 receptors, and has good reproducibility of striatal D_2 bindings (Volkow et al., 1993). Because the density of extrastriatal D_2 receptors is less than one-tenth of striatal D_2 receptors (Ito et al., 2008), [^{11}C]raclopride is suitable for the evaluation of striatal D_2 receptors, but not of extrastriatal D_2 receptors, due to its moderate affinity for D_2 receptors. Dynamic scans were performed for 60 min. All emission scans were reconstructed with a Hanning filter cutoff frequency of 0.4 (full width at half maximum, 7.5 mm). MRI was performed on Gyroscan NT (Philips Medical Systems) (1.5 T). T1-weighted images of the brain were obtained for all subjects. Scan parameters were 1-mm-thick, three-dimensional T1 images with a transverse plane (repetition time/echo time, 19/10 ms; flip angle, 30°; scan matrix, 256 × 256 pixels; field of view, 256 × 256 mm; number of excitations, 1).

Quantification of D_1 and D_2 receptors

Because one subject felt discomfort from the head fixation device during the [^{11}C]FLB457 scan, the scan was discontinued and the data of this subject were excluded from the subsequent analysis. Quantitative analysis was performed using the three-parameter simplified reference tissue model (Lammertsma and Hume, 1996; Olsson et al., 1999). This method is well established for [^{11}C]SCH23390, [^{11}C]FLB457 and [^{11}C]raclopride (Lammertsma and Hume, 1996; Olsson et al., 1999) and is widely used (Aalto et al., 2005; Takahashi et al., 2008; McNab et al., 2009; Takahashi et al., 2010), and it allows us to quantify DA receptors without arterial blood sampling, an invasive and time-consuming procedure. The cerebellum was used as reference region because it has been shown to be almost devoid of D_1 and D2 receptors (Farde et al., 1987; Suhara et al., 1999). The model provides an estimation of the binding potential [$BP_{ND\ (nondisplaceable)}$] (Innis et al., 2007), which is defined by the following equation: $BP_{ND} = k_3/k_4 = f_2 B_{max}/\{K_d [1 + \Sigma_i F_i/K_{di}]\}$, where k_3 and k_4 describe the bidirectional exchange of tracer between the free compartment and the compartment representing specific binding, f_2 is the "free fraction" of nonspecifically bound radioligand in brain, B_{max} is the receptor density, K_d is the equilibrium dissociation constant for the radioligand, and F_i and K_{di} are the free concentration and the dissociation constant of competing ligands, respectively (Lammertsma and Hume, 1996). Based on this model, we created parametric images of BP_{ND} using the basis function method (Gunn et al., 1997) to conduct voxelwise statistical parametric mapping (SPM) analysis.

In addition to the SPM analysis, we conducted region-of-interest (ROI) analysis. The tissue concentrations of the radioactivities of [^{11}C]SCH23390, [^{11}C]FLB457 and [^{11}C]raclopride were obtained from anatomically defined ROIs. The individual MRIs were coregistered on [^{11}C]SCH23390, [^{11}C]FLB457 and [^{11}C]raclopride PET images of summated activity for 60, 90 and 60 min, respectively. The ROIs were defined on coregistered MRI with reference to the brain atlas. Given our hypothesis from the previous literature (Hsu et al., 2009), the ROIs were set on the striatum (caudate and putamen). Manual delineation of caudate and putamen ROIs was based on the dorsal caudate and dorsal putamen criteria, respectively, of Mawlawi et al. (2001). The average values of right and left ROIs were used to increase the signal-to-noise ratio for the calculations.

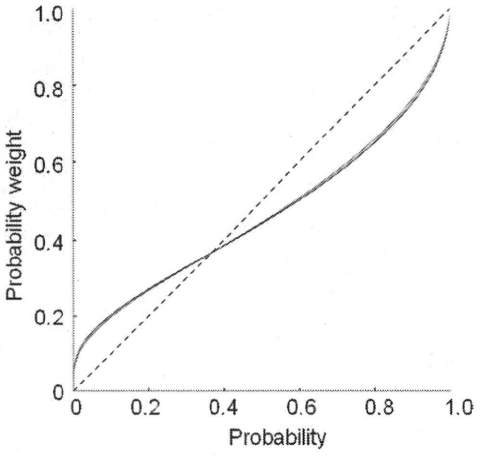

Figure 1. The fitted probability weighting function with the Prelec model. The red line represents the first group ($N = 18$ subjects) with D_1 receptors and extrastriatal D_2 receptors investigated. The black line is the second group ($N = 18$ subjects) whose striatal D_2 receptors were investigated.

Statistical analysis

SPM analysis. Parametric images of BP_{ND} of [^{11}C]SCH23390, [^{11}C]FLB457 and [^{11}C]raclopride were analyzed using the SPM2 software package (Wellcome Department of Cognitive Neurology, London, UK) running with MATLAB (MathWorks). Parametric images of BP_{ND} were normalized into MNI (Montreal Neurological Institute) template space. Normalized BP_{ND} images were smoothed with a Gaussian filter to 8 mm full-width half-maximum. Using each of the individual behavioral parameters (α and σ) as covariate, regression analyses with the BP_{ND} images and the covariates were performed. A statistical threshold of $p < 0.05$ corrected for multiple comparisons across the whole brain was used, except for a priori hypothesized regions, which were thresholded at $p < 0.001$ uncorrected ($r > 0.68$) for examination of effect size (only clusters involving 10 or more contiguous voxels are reported). These a priori ROIs included the caudate and putamen.

ROI analysis. Pearson's correlation coefficients between BP_{ND} of [^{11}C]SCH23390 and [^{11}C]raclopride in the ROIs and behavioral parameters (α and σ) were calculated using SPSS software. Because some subjects were smokers, we further calculated partial correlation coefficients between BP_{ND} of [^{11}C]SCH23390 and [^{11}C]raclopride and behavioral parameters to control for the potential influence of smoking (number of cigarettes per day).

Results

In the first group, with D_1 receptors and extrastriatal D_2 receptors investigated, the mean (SD) α of the weighting function and σ of the utility function were 0.58 (0.16) and 0.99 (0.33), respectively. The second group, in which striatal D_2 receptors were investigated, the mean (SD) α and σ were 0.56 (0.19) and 0.98 (0.18), respectively, indicating that the two groups were comparable. Averaged weighting functions and value functions of the two groups are shown in Figure 1 and supplemental Figure 3 (available at www.jneurosci.org as sup-

plemental material), respectively. Normalized parametric images of BP_{ND} of [^{11}C]SCH23390, [^{11}C]raclopride and [^{11}C]FLB457 are shown in Figure 2*A*, *B*, and *C*, respectively. The mean BP_{ND} values of [^{11}C]SCH23390 in the caudate and putamen were 1.86 ± 0.24 and 2.01 ± 0.22, and those of [^{11}C]raclopride were 3.00 ± 0.32 and 3.61 ± 0.37, respectively. Voxel-by-voxel SPM analysis revealed significant positive correlation ($r > 0.68$, $p < 0.001$) between striatal D_1 receptor binding and the nonlinearity parameter α of weighting function [right striatum, peak (30, −8, −4), 230 voxels; left striatum, peak (−20, −4, 8), 154 voxels] (Fig. 3*A*). Independent ROI analyses revealed that D_1 receptor binding in the putamen showed a significant correlation with α (Fig. 3*B*; Table 1), and D_1 receptor binding in the caudate showed a trend level correlation with α (Table 1). That is, people with lower striatal D_1 receptor binding tend to be more risk-seeking for low probability gambles and more risk-averse for high probability gambles. SPM analysis showed that extrastriatal D_1 binding was not correlated with α. SPM and ROI analyses revealed that neither striatal nor extrastriatal D_2 receptor binding was correlated with α. None of [^{11}C]SCH23390, [^{11}C]FLB457 and [^{11}C]raclopride binding was correlated with the power σ of the value function. Correlation analyses with controlling for the potential influence of smoking revealed identical results, indicating that the influence of smoking was minimal. The results of partial correlation analyses of ROIs between behavioral parameters (α and σ) and BP_{ND} values of [^{11}C]SCH23390 and [^{11}C]raclopride in the striatum after controlling for the potential influence of smoking are summarized in supplemental Table 2, available at www.jneurosci.org as supplemental material.

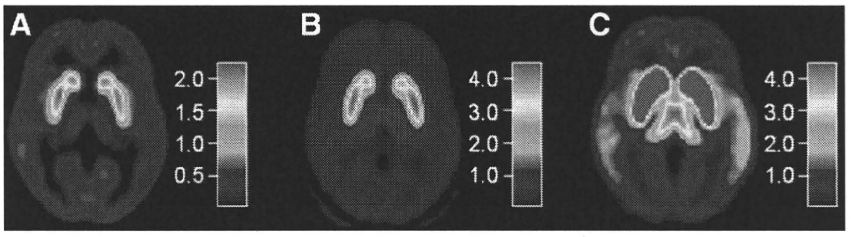

Figure 2. Maps of DA D_1 and D_2 BP, averaged across participants (axial slices at the level of $Z = 0$ of MNI coordinates). ***A***, D_1 BP, measured with [^{11}C]SCH23390 ($N = 18$ subjects). ***B***, Striatal D_2 BP, measured with [^{11}C]raclopride ($N = 18$ subjects). ***C***, Extrastriatal D_2 BP, measured with [^{11}C]FLB457 ($N = 17$ subjects). Although [^{11}C]FLB457 accumulates to a high degree in the striatum, striatal data were not evaluated because the duration of the [^{11}C]FLB457 PET study was not sufficient to obtain equilibrium in the striatum. The bar indicates the range of BP.

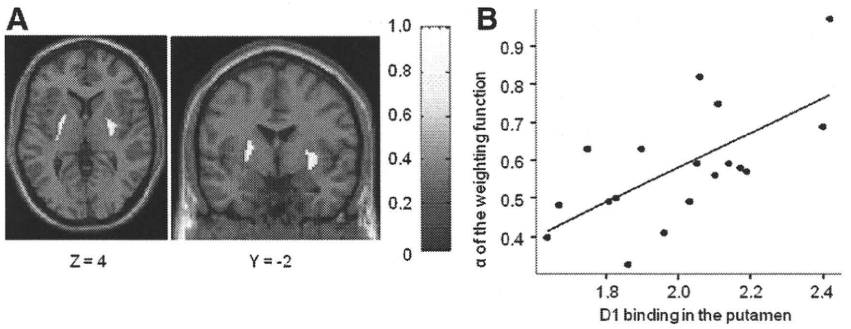

Figure 3. Correlation between nonlinearity of probabilities weighting and D_1 binding in the striatum ($N = 18$ subjects). ***A***, Image showing regions of correlation between nonlinearity parameter of weighting function and D_1 binding in the striatum. The bar shows the range of the correlation coefficient. ***B***, Plots and regression line of correlation between α (nonlinearity parameter) and binding potential of the putamen ($r = 0.66$, $p = 0.003$).

Table 1. Correlation between behavioral parameters (α and σ) and BP_{ND} values of [^{11}C]SCH23390 ($N = 18$ subjects) and [^{11}C]raclopride ($N = 18$ subjects) in the striatum

	α	σ
D_1 receptors		
Caudate	0.011 ($r = 0.582$)	0.717 ($r = 0.092$)
Putamen	0.003* ($r = 0.658$)	0.260 ($r = 0.280$)
D_2 receptors		
Caudate	0.305 ($r = 0.256$)	0.218 ($r = 0.305$)
Putamen	0.242 ($r = 0.291$)	0.122 ($r = 0.378$)

p values (correlation coefficients) are shown. *$p < 0.01$.

Discussion

We provided the first evidence of a relation between striatal D_1 receptor binding and nonlinear probability weighting during decision-making under risk. Based on circumstantial evidence (Kuhnen and Knutson, 2005; Wittmann et al., 2008) and a speculative review (Trepel et al., 2005), it has been suggested that curvature of the weighting function might be modulated by DA transmission. Utilizing a molecular imaging technique, we directly measured the relation between DA receptors and the nonlinearity of weighting function *in vivo*. Individuals with lower striatal D_1 receptor binding showed more nonlinear probability weighting and more pronounced overestimation of low probabilities and underestimation of high probabilities. Low D_1 receptor binding means that available receptors for phasically released DA are limited. In such case, phasic DA release in response to positive outcomes can stimulate limited D_1 receptors in the striatum. In contrast, low-level baseline tonic DA release is enough for stimulating D_2 receptors (Frank et al., 2007; Schultz, 2007). Therefore, the variability of D_2 receptor binding might have less impact on current behavioral task during which phasic DA release occurs in response to reward cue.

This molecular imaging approach allows us to broaden our understanding of the neurobiological mechanism underlying nonlinear weighting beyond the current knowledge attained by neuroeconomics fMRI. An fMRI study using a value-titration paradigm has shown that differential anterior cingulate activation during estimation of high probabilities relative to low probabilities was positively correlated with Prelec's nonlinearity parameter α across subjects (Paulus and Frank, 2006). Another fMRI study with risks of electric shocks found similar nonlinear response in the caudate/subgenual anterior cingulate (Berns et al., 2008). More recently, Hsu et al. (2009), using a simpler exposure-choice paradigm, demonstrated that Prelec's nonlinearity parameter α was negatively correlated with striatal activity during reward anticipation under risk. That is, people with a greater degree of nonlinearity in striatal activation to anticipated reward tend to overestimate low probabilities (to be risk-seeking) and underestimate high probabilities (to be risk-averse).

Exploring novelty and risk-seeking behavior are, to some extent, desirable and advantageous for the survival and develop-

ment of many species including human (Kelley et al., 2004). Being too risk-averse would lose opportunities to obtain possibly better outcomes. However, excessive risk-seeking may contribute to reckless choices such as initiation of drug use (or gambling) and transition to regular drug use (or gambling) (Kreek et al., 2005). Pathological gambling and drug addiction frequently co-occur, and it is suggested that the neurobiological mechanisms underlying the two conditions overlap (Tamminga and Nestler, 2006; Steeves et al., 2009). In fact, pharmacological therapy for drug addiction has been shown to also be effective when applied to pathological gambling (Tamminga and Nestler, 2006). Animal studies demonstrated that stimulation of D_1 receptors by a selective agonist increased risky choice and blockade of D_1 receptors decreased risky choice in rats. Although D_2 agonist/antagonist showed similar actions, their effects were not as pronounced as those of D_1 agonist/antagonist (St Onge and Floresco, 2009). A human genetic study reported that variants of the gene for D_1 receptors were linked to risky and novelty-seeking behaviors (Comings et al., 1997), although the genes for other subtypes of DA receptors are also linked to those behaviors. More recently, a PET study suggested that reduced D_1 receptor binding may be associated with an increased risk of relapse in drug addiction (Martinez et al., 2009).

The curvature of the weighting function is traditionally explained by the psychophysics of diminishing sensitivity, the idea that sensitivity to changes in probability decreases as probability moves away from the endpoints of 0 and 1 (Tversky and Kahneman, 1992). However, it has also been suggested that emotional responses to gambles influence weighting as well. In particular, the overweighting of low-probability gains may reflect hope of winning and the underweighting of high-probability gains may reflect fear of losing a "near sure thing" (Trepel et al., 2005). One study supportive of this hypothesis found more nonlinear weighting functions for gambles over emotional outcomes (kisses and shocks) than over money (Rottenstreich and Hsee, 2001). In this sense, individuals with lower striatal D_1 binding might be interpreted as showing more "emotional" decision-making.

We used a simple behavioral task with only positive outcomes to estimate weighting function in this study. Any generalization of our findings needs to be approached with caution. We make more complex decisions in the real world where both positive and negative outcomes are possible, and have to pay attention to relative differences in the magnitude of gains and losses. A computational model has suggested that tonic D_2 receptor stimulation in the striatum inhibits response to avoid negative outcomes (Frank et al., 2007), and other neurotransmitters such as serotonin and noradrenaline are thought to be involved in the complex decision-making process (Trepel et al., 2005; Frank et al., 2007; Cools et al., 2008; Doya, 2008). Using behavioral tasks with negative outcomes, future studies to investigate involvements of other neurotransmissions as well as other areas that are related to punishment or negative emotions such as the orbitofrontal cortex, insula and amygdala (Trepel et al., 2005; Pessiglione et al., 2006; Voon et al., 2010) are recommended. Furthermore, our subjects were relatively homogeneous in terms of economic status (the majority were students). Our findings might not be representative of various samples with different background and socioeconomic status. Notwithstanding this limitation, the present study illustrated that molecular imaging can provide a new research direction for neuroeconomics and decision-making studies by more directly investigating the association between striatal DA transmission and nonlinear probability weighting. This approach may shed light on neurotransmission effects on emotional and boundedly rational decision-making in our daily life. At the same time, understanding the molecular mechanism of extreme or impaired decision-making can contribute to the assessment and prevention of drug and gambling addiction and the development of novel pharmacological therapies for those addictions.

References

Aalto S, Brück A, Laine M, Någren K, Rinne J (2005) Frontal and temporal dopamine release during working memory and attention tasks in healthy humans: a positron emission tomography study using the high-affinity dopamine D2 receptor ligand [^{11}C] FLB 457. J Neurosci 25:2471–2477.

Berns GS, Capra CM, Chappelow J, Moore S, Noussair C (2008) Nonlinear neurobiological probability weighting functions for aversive outcomes. Neuroimage 39:2047–2057.

Camerer C, Loewenstein G (2004) Behavioral economics: past, present, future. In: Advances in behavioral economics (Camerer C, Loewenstein G, Rabin M, eds), pp 3–51. Princeton: Princeton UP.

Comings D, Gade R, Wu S, Chiu C, Dietz G, Muhleman D, Saucier G, Ferry L, Rosenthal RJ, Lesieur HR, Rugle LJ, MacMurray P (1997) Studies of the potential role of the dopamine D1 receptor gene in addictive behaviors. Mol Psychiatry 2:44–56.

Cools R, Roberts AC, Robbins TW (2008) Serotoninergic regulation of emotional and behavioural control processes. Trends Cogn Sci 12:31–40.

De Martino B, Kumaran D, Seymour B, Dolan RJ (2006) Frames, biases, and rational decision-making in the human brain. Science 313:684–687.

Doya K (2008) Modulators of decision making. Nat Neurosci 11:410–416.

Ekelund J, Slifstein M, Narendran R, Guillin O, Belani H, Guo NN, Hwang Y, Hwang DR, Abi-Dargham A, Laruelle M (2007) In vivo DA D1 receptor selectivity of NNC 112 and SCH 23390. Mol Imaging Biol 9:117–125.

Farde L, Halldin C, Stone-Elander S, Sedvall G (1987) PET analysis of human dopamine receptor subtypes using 11C-SCH 23390 and 11C-raclopride. Psychopharmacology (Berl) 92:278–284.

Fox C, Poldrack R (2009) Prospect theory and the brain. In: Neuroeconomics (Glimcher PW, Camerer C, Fehr E, Poldrack R, eds), pp 145–174. London: Academic.

Frank MJ, Scheres A, Sherman SJ (2007) Understanding decision-making deficits in neurological conditions: insights from models of natural action selection. Philos Trans R Soc Lond B Biol Sci 362:1641–1654.

Grace A (1991) Phasic versus tonic dopamine release and the modulation of dopamine system responsivity: a hypothesis for the etiology of schizophrenia. Neuroscience 41:1–24.

Gunn RN, Lammertsma AA, Hume SP, Cunningham VJ (1997) Parametric imaging of ligand-receptor binding in PET using a simplified reference region model. Neuroimage 6:279–287.

Hirvonen J, Någren K, Kajander J, Hietala J (2001) Measurement of cortical dopamine d1 receptor binding with 11C [SCH23390]: a test-retest analysis. J Cereb Blood Flow Metab 21:1146–1150.

Hsu M, Krajbich I, Zhao C, Camerer CF (2009) Neural response to reward anticipation under risk is nonlinear in probabilities. J Neurosci 29:2231–2237.

Innis RB, Cunningham VJ, Delforge J, Fujita M, Gjedde A, Gunn RN, Holden J, Houle S, Huang SC, Ichise M, Iida H, Ito H, Kimura Y, Koeppe RA, Knudsen GM, Knuuti J, Lammertsma AA, Laruelle M, Logan J, Maguire RP, et al (2007) Consensus nomenclature for in vivo imaging of reversibly binding radioligands. J Cereb Blood Flow Metab 27:1533–1539.

Ito H, Takahashi H, Arakawa R, Takano H, Suhara T (2008) Normal database of dopaminergic neurotransmission system in human brain measured by positron emission tomography. Neuroimage 39:555–565.

Kelley AE, Schochet T, Landry CF (2004) Risk taking and novelty seeking in adolescence: introduction to part I. Ann N Y Acad Sci 1021:27–32.

Kreek MJ, Nielsen DA, Butelman ER, LaForge KS (2005) Genetic influences on impulsivity, risk taking, stress responsivity and vulnerability to drug abuse and addiction. Nat Neurosci 8:1450–1457.

Kuhnen CM, Knutson B (2005) The neural basis of financial risk taking. Neuron 47:763–770.

Lammertsma AA, Hume SP (1996) Simplified reference tissue model for PET receptor studies. Neuroimage 4:153–158.

Lattimore P, Baker J, Witte A (1992) The influence of probability on risky choice: a parametric examination. Behav Organ 17:377–400.

Leyton M, Boileau I, Benkelfat C, Diksic M, Baker G, Dagher A (2002) Amphetamine-induced increases in extracellular dopamine, drug want-

ing, and novelty seeking: a PET/[11C] raclopride study in healthy men. Neuropsychopharmacology 27:1027–1035.

Martinez D, Slifstein M, Narendran R, Foltin RW, Broft A, Hwang DR, Perez A, Abi-Dargham A, Fischman MW, Kleber HD, Laruelle M (2009) Dopamine D1 receptors in cocaine dependence measured with PET and the choice to self-administer cocaine. Neuropsychopharmacology 34:1774–1782.

Mawlawi O, Martinez D, Slifstein M, Broft A, Chatterjee R, Hwang DR, Huang Y, Simpson N, Ngo K, Van Heertum R, Laruelle M (2001) Imaging human mesolimbic dopamine transmission with positron emission tomography: I. accuracy and precision of D2 receptor parameter measurements in ventral striatum. J Cereb Blood Flow Metab 21:1034–1057.

McNab F, Varrone A, Farde L, Jucaite A, Bystritsky P, Forssberg H, Klingberg T (2009) Changes in cortical dopamine D1 receptor binding associated with cognitive training. Science 323:800–802.

Olsson H, Halldin C, Swahn CG, Farde L (1999) Quantification of [^{11}C]FLB 457 binding to extrastriatal dopamine receptors in the human brain. J Cereb Blood Flow Metab 19:1164–1173.

Paulus MP, Frank LR (2006) Anterior cingulate activity modulates nonlinear decision weight function of uncertain prospects. Neuroimage 30:668–677.

Pessiglione M, Seymour B, Flandin G, Dolan RJ, Frith CD (2006) Dopamine-dependent prediction errors underpin reward-seeking behaviour in humans. Nature 442:1042–1045.

Prelec D (1998) The probability weighting function. Econometrica 66: 497–527.

Rangel A, Camerer C, Montague PR (2008) A framework for studying the neurobiology of value-based decision making. Nat Rev Neurosci 9:545–556.

Rottenstreich Y, Hsee CK (2001) Money, kisses, and electric shocks: on the affective psychology of risk. Psychol Sci 12:185–190.

Schultz W (2007) Behavioral dopamine signals. Trends Neurosci 30:203–210.

Steeves TD, Miyasaki J, Zurowski M, Lang AE, Pellecchia G, Van Eimeren T, Rusjan P, Houle S, Strafella AP (2009) Increased striatal dopamine release in Parkinsonian patients with pathological gambling: a [^{11}C] raclopride PET study. Brain 132:1376–1385.

St Onge JR, Floresco SB (2009) Dopaminergic modulation of risk-based decision making. Neuropsychopharmacology 34:681–697.

Sudo Y, Suhara T, Inoue M, Ito H, Suzuki K, Saijo T, Halldin C, Farde L (2001) Reproducibility of [^{11}C]FLB 457 binding in extrastriatal regions. Nucl Med Commun 22:1215–1221.

Suhara T, Sudo Y, Okauchi T, Maeda J, Kawabe K, Suzuki K, Okubo Y, Nakashima Y, Ito H, Tanada S, Halldin C, Farde L (1999) Extrastriatal dopamine D2 receptor density and affinity in the human brain measured by 3D PET. Int J Neuropsychopharmcol 2:73–82.

Takahashi H, Kato M, Takano H, Arakawa R, Okumura M, Otsuka T, Kodaka F, Hayashi M, Okubo Y, Ito H Suhara T (2008) Differential contributions of prefrontal and hippocampal dopamine D1 and D2 receptors in human cognitive functions. J Neurosci 28:12032–12038.

Takahashi H, Takano H, Kodaka F, Arakawa R, Yamada M, Otsuka T, Hirano Y, Kikyo H, Okubo Y, Kato M, Obata T, Ito H, Suhara T (2010) Contribution of dopamine D1 and D2 receptors to amygdala activity in human. J Neurosci 30:3043–3047.

Tamminga CA, Nestler EJ (2006) Pathological gambling: focusing on the addiction, not the activity. Am J Psychiatry 163:180–181.

Tom SM, Fox CR, Trepel C, Poldrack RA (2007) The neural basis of loss aversion in decision-making under risk. Science 315:515–518.

Trepel C, Fox CR, Poldrack RA (2005) Prospect theory on the brain? Toward a cognitive neuroscience of decision under risk. Brain Res Cogn Brain Res 23:34–50.

Tversky A, Kahneman D (1992) Advances in prospect theory: cumulative representation of uncertainty. J Risk Uncertain 5:297–323.

Volkow ND, Fowler JS, Wang GJ, Dewey SL, Schlyer D, MacGregor R, Logan J, Alexoff D, Shea C, Hitzemann R, Angrist B, Wolf AP (1993) Reproducibility of repeated measures of carbon-11-raclopride binding in the human brain. J Nucl Med 34:609–613.

von Neumann J, Morgenstern O (1944) Theory of games and economic behavior. Princeton: Princeton UP.

Voon V, Pessiglione M, Brezing C, Gallea C, Fernandez HH, Dolan RJ, Hallett M (2010) Mechanisms underlying dopamine-mediated reward bias in compulsive behaviors. Neuron 65:135–142.

Wittmann BC, Daw ND, Seymour B, Dolan RJ (2008) Striatal activity underlies novelty-based choice in humans. Neuron 58:967–973.

Wu G, Gonzalez R (1996) Curvature of the probability weighting function. Manage Sci 42:1676–1690.

Zack M, Poulos CX (2004) Amphetamine primes motivation to gamble and gambling-related semantic networks in problem gamblers. Neuropsychopharmacology 29:195–207.

Schizophrenia Bulletin vol. 36 no. 3 pp. 642–647, 2010
doi:10.1093/schbul/sbn132
Advance Access publication on October 16, 2008

Functional Deficits in the Extrastriate Body Area During Observation of Sports-Related Actions in Schizophrenia

Hidehiko Takahashi[1–3], Motoichiro Kato[4], Takeshi Sassa[5], Tomohisa Shibuya[5,6], Michihiko Koeda[7], Noriaki Yahata[8], Masato Matsuura[3], Kunihiko Asai[5], Tetsuya Suhara[2], and Yoshiro Okubo[7]

[2]Department of Molecular Neuroimaging, Molecular Imaging Center, National Institute of Radiological Sciences, 9-1, 4-chome, Anagawa,Inage-ku, Chiba 263-8555, Japan; [3]Department of Life Sciences and Bio-informatics, Graduate School of Health Sciences, Tokyo Medical and Dental University, 1-5-45 Yushima Bunkyo-ku, Tokyo 113-8549, Japan; [4]Department of Neuropsychiatry, Keio University School of Medicine, 35 Shinanomachi, Shinjuku-ku, Tokyo 160-8582, Japan; [5]Department of Psychiatry, Asai Hospital, 38-1 Katoku Togane 283-8650, Japan; [6]Department of Human Sciences, Toyo Gakuen University, 1-26-3, Hongo, Bunkyo-ku, Tokyo 113-0033, Japan; [7]Department of Neuropsychiatry and [8]Department of Pharamacology, Nippon Medical School, 1-1-5, Sendagi, Bunkyo-ku, Tokyo 113-8603, Japan

Exercise and sports are increasingly being implemented in the management of schizophrenia. The process of action perception is as important as that of motor execution for learning and acquiring new skills. Recent studies have suggested that body-selective extrastriate body area (EBA) in the posterior temporal-occipital cortex is involved not only in static visual perception of body parts but also in the planning, imagination, and execution of actions. However, functional abnormality of the EBA in schizophrenia has yet to be investigated. Using functional magnetic resonance imaging (fMRI) with a task designed to activate the EBA by sports-related actions, we aimed to elucidate functional abnormality of the EBA during observation of sports-related actions in patients with schizophrenia. Twelve schizophrenia patients and 12 age-sex–matched control participants participated in the study. Using sports-related motions as visual stimuli, we examined brain activations during observation of context-congruent actions relative to context-incongruent actions by fMRI. Compared with controls, the patients with schizophrenia demonstrated diminished activation in the EBA during observation of sports-related context-congruent actions. Furthermore, the EBA activation in patients was negatively correlated with the severity of negative and general psychopathology symptoms measured by the Positive and Negative Syndrome Scale. Dysfunction of the EBA might reflect a difficulty in representing dynamic aspects of human actions and possibly lead to impairments of simulation, learning, and execution of actions in schizophrenia.

Key words: body/extrastriate body area/schizophrenia/sports/exercise/fMRI

Introduction

With the introduction of atypical antipsychotics, awareness of these comorbid metabolic disturbances in schizophrenia has become considerably increased among many health care professionals and patients.[1] For the management of comorbid metabolic disturbances, exercise is one of the most acknowledged interventions.[2] At the same time, exercise and sports have been recognized as having a positive impact on the treatment and rehabilitation of schizophrenia.[3] However, individuals living with schizophrenia are less physically active than the general population.[4,5] Moreover, they generally show psychomotor poverty and clumsiness[6] and have an impairment of motor skill learning,[7,8] which have been suggested to be linked to a dysfunctional motor execution system including the striatum-frontal-cerebellum.[9,10]

It is widely documented in psychological and neurocognitive studies that the systems that mediate action perception, imitation, planning, and execution overlap and interact with each other.[11,12] These studies have supported the view that when we observe others' actions, observed action is automatically simulated and matched with internal motor representation and could even be imitated unconsciously (Chameleon effect).[12,13] These externally triggered motor representations are then used to understand, learn, and reproduce the observed behavior.[14] Therefore, for learning and acquiring new skills, the process of action perception is as important as that of motor execution.

Passive viewing of biological motions has been known to activate the superior temporal sulcus (STS),[15] and the STS has been suggested to have a more extended function in social cognition such as detecting intention of

[1]To whom correspondence should be addressed; tel: +81-43-206-3251, fax: +81-43-253-0396, e-mail: hidehiko@nirs.go.jp.

others.[16,17] Kim et al[18] reported that schizophrenia patients were impaired in the perception of biological motion, and they predicted that impaired biological motion processing arises from functional deficit in the STS. Although the STS is a central node of processing biological motion, passive viewing of biological motion has consistently activated the posterior temporal-occipital cortex including the body-selective extrastriate body area (EBA)[19] in close proximity to the STS.[20] Originally, the EBA was identified as an area that responds selectively to static human bodies and body parts.[19] In biological motion tasks, low-level visual stimuli such as random moving dots have been used as control task, which make it difficult to clarify whether the EBA is only involved in body-sensitive early visual processing or is participant as a part of a system for inferring the action and intention of others like the STS. However, recent studies have suggested an extended role for the EBA, involving not only static visual perception of body parts but also the planning, imagination, and execution of actions.[21,22] In addition, we have shown that sports-related context-congruent actions produced greater activation in the EBA, along with the STS, than context-incongruent actions.[23] Compared with frontal or limbic areas, the posterior temporal-occipital or temporal-parietal cortex has received relatively little attention in the field of schizophrenia research,[24] and functional abnormality of the EBA in schizophrenia has yet to be investigated. We hypothesized that patients with schizophrenia would show diminished activation in the EBA, along with the STS, in response to sports-related context-congruent actions.

Methods

Participants Twelve patients with schizophrenia (6 men and 6 women, mean age: 31.8 ± 7.2 [SD] years) were studied. Diagnoses were based on the Structured Clinical Interview for *Diagnostic and Statistical Manual of Mental Disorders, Fourth Edition,* Axis I Disorders. All patients were attending the day hospital unit of Asai Hospital. Exclusion criteria were current or past substance abuse and a history of alcohol-related problems, mood disorder, or organic brain disease. The mean illness duration was 9.8 ± 6.9 years. All patients received antipsychotics (mean chlorpromazine equivalent daily dosage = 641.6 ± 471.2 mg).[25,26] Clinical symptoms were assessed by the Positive and Negative Syndrome Scale (PANSS) for schizophrenia.[27] Mean total scores of PANSS and subscale (positive scale, negative scale, and general psychopathology scale) were 69.8 ± 13.6, 14.3 ± 4.0, 19.7 ± 4.7, and 35.8 ± 6.4, respectively. The ratings were reviewed by trained senior psychiatrists, H.T. and T.S., after the patient interviews, and disagreements were resolved by consensus; consensus ratings were used in this study. Twelve age-sex–matched normal controls (6 men and 6 women, mean age 29.4 ± 4.5 years) were recruited from the surrounding community. The candidates were carefully screened, and standardized interviews were conducted by H.T. and T.S.. They did not meet criteria for any psychiatric disorders. None of the controls were taking alcohol or medication at the time, nor did they have a history of psychiatric disorder, significant physical illness, neurological disorder, or alcohol or drug dependence. All subjects were right-handed, and they all underwent a magnetic resonance imaging (MRI) to rule out cerebral anatomic abnormalities. All subjects had achieved an educational level of high school or higher. All of them had the experience of playing basketball in elementary school or junior high school, but they had little opportunity, if any, to play basketball thereafter. After complete explanation of the study, written informed consent was obtained from all participants, and the study was approved by the Ethics Committee of Asai Hospital.

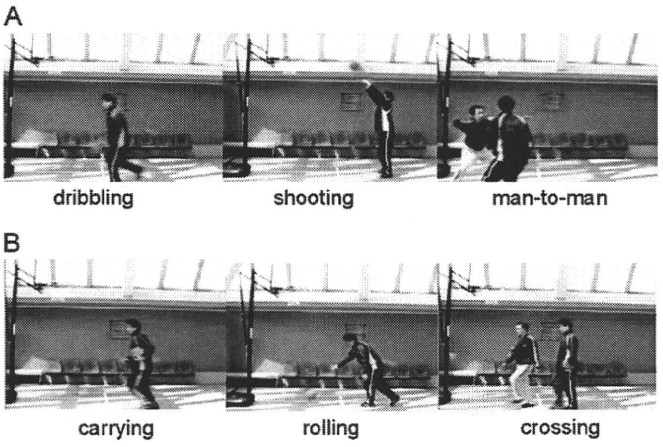

Fig. 1. Sample of Still Frames From Video Clips. A, Basketball-related motions; B, basketball-unrelated motions.

Materials

We employed the same visual stimuli as in the previous report where healthy volunteers were studied. The stimuli were designed to activate the EBA by sports-related actions.[23] Two types of video clips were provided (basketball-related motions [BRM] and basketball-unrelated motions [BUM]). Examples of the video clips are shown in figure 1. BRM consisted of 3 types of scenes (player shooting a free throw, player dribbling, 2 players performing man-to-man defense/offense). BUM also consisted of 3 types of scenes (player rolling a basketball, player carrying a basketball, and one person crossing in front of another without interaction). In order to make BRM and BUM as similar as possible, all players in the video clips performed in front of a basket hoop on a basketball court, and the number of persons, objects, motion direction, and speed were matched, ie, rolling a basketball, carrying a basketball, and crossing in front of another without interaction corresponded to shooting a free throw, dribbling, and man-to-man defense,

respectively. The video clips were projected via computer onto a screen mounted on a head coil. The subjects were instructed to pay attention to the video clips and to press a selection button with the right index finger when they watched the free throw scene and the basketball-rolling scene, indicating that they had paid attention to them. The experimental design consisted of 5 blocks for each of the 2 conditions (BRM and BUM) interleaved with 20-second rest periods. During the rest condition, participants viewed a crosshair pattern projected to the center of the screen. In the BRM and BUM 24-second blocks, 3 scenes were presented twice for 4 seconds each.

Image Acquisition

Images were acquired with a 1.5-T Signa system (General Electric, Milwaukee, WI). Functional images of 115 volumes were acquired with T2*-weighted gradient echo planar imaging sequences sensitive to blood oxygenation level–dependent contrast. Each volume consisted of 40 transaxial contiguous slices with a slice thickness of 3 mm to cover almost the whole brain (flip angle, 90°; echo time (TE), 50 ms; repetition time (TR), 4 sec; matrix, 64 × 64; field of view, 24 × 24 cm). High-resolution, T1-weighted anatomic images were acquired for anatomic comparison (124 contiguous axial slices; 3D Spoiled-Grass sequence; slice thickness, 1.5 mm; TE, 9 ms; TR, 22 ms; flip angle, 30°; matrix, 256 × 192; field of view, 25 × 25 cm).

Analysis of Functional Imaging Data

Data analysis was performed with SPM02 (Wellcome Department of Cognitive Neurology, London, UK). All volumes were realigned to the first volume of each session to correct for subject motion and were spatially normalized to the Montreal Neurological Institute template. Functional images were spatially smoothed with a 3D isotropic Gaussian kernel (full width at half maximum of 8 mm). Significant hemodynamic changes for each condition were examined using the general linear model with boxcar functions convolved with a hemodynamic response function. Statistical parametric maps for each contrast of the t statistic were calculated on a voxel-by-voxel basis.

To examine possible group differences in response to BUM (baseline), we conducted a 2-sample t test of BUM contrast. To assess the specific condition effect, we used the contrasts of BRM minus BUM. A random-effects model was implemented for group analysis. A 1-sample t test was applied to determine group activation for the contrasts of BRM minus BUM. Between-group comparison of BRM minus BUM contrast was performed with a 2-sample t test. We used SPM's small volume correction to correct for multiple testing in regions about which we had a priori hypotheses. These a priori volumes of interest (VOIs) included the EBA (inferior temporal cortex) and STS (superior temporal cortex). VOIs were defined by standardized VOI templates implemented in brain atlas software.[28] Significant differences surviving this correction at $P < .05$ were determined as were activations outside regions of interest surviving a threshold of $P < .001$, uncorrected, with an extent threshold of 10 contiguous voxels.

We conducted regression analyses to demonstrate a link between regional brain activities with the patients' demographics. Using the demographic data (age, duration of illness, chlorpromazine equivalent daily dosage, and PANSS scores) for each subject as covariates, regression analyses with the BRM minus BUM contrasts and the covariates were performed at the second level. The same threshold as used in the between-group comparison was applied. To confine the regions where significant group differences were observed, we created masks of group differences of the BRM minus BUM contrast from the 2-sample t test (threshold at $P < .05$, uncorrected), and these masks were applied inclusively. Using the effect sizes, representing the percent signal changes, of the BRM minus BUM contrasts at the peak coordinates uncovered in the regression analyses, we plotted the functional MRI (fMRI) signal changes and PANSS scores.

Results

Behavioral Data

All patients and controls paid attention to the video clips and pressed the button appropriately (accuracy was virtually 100%).

fMRI Results

In the control group, BRM minus BUM condition produced activations in the bilateral posterior temporal-occipital cortex including the bilateral EBA ($x = 58$, $y = -60$, $z = 2$; $t = 4.86$), middle temporal ($x = 54$, $y = -66$, $z = -12$; $t = 8.38$), right STS ($x = 56$, $y = -22$, $z = -2$; $t = 6.58$), bilateral premotor cortex ($x = -48$, $y = -4$, $z = 40$; $t = 4.94$), and bilateral inferior parietal lobules ($x = -34$, $y = -50$, $z = 54$; $t = 7.25$) (coordinates and t score refer to the peak of each brain region). In the patient group, BRM minus BUM condition produced activations in the left lingual gyrus ($x = -6$, $y = 92$, $z = 0$; $t = 6.52$), right prefrontal cortex ($x = 36$, $y = 52$, $z = 14$; $t = 5.66$), and right premotor cortex ($x = 36$, $y = -2$, $z = 54$; $t = 4.52$).

A 2-sample t test revealed no significant differences (threshold at $P < .001$, uncorrected) in the activations by BUM between controls and patients. Group comparison of the BRM minus BUM contrast showed that patients demonstrated significantly less activation in the bilateral EBA, bilateral parahippocampal gyrus, right STS, right temporal pole, right lingual gyrus, and globus pallidus (table 1 and figure 2). The activations in a priori regions (EBA and STS) survived a threshold of $P < .05$

Table 1. Regions showing diminished activation in response to BRM-BUM condition in 12 patients with schizophrenia compared with 12 controls

Brain regions	R/L	MNI coordinates			BA	*t* value	voxels
		x	*y*	*z*			
EBA (MTG)*	L	−40	−60	−4	37	5.37	106
EBA (MTG)*	R	52	−68	6	37	5.08	74
STS (STG)*	R	54	−22	0	21, 22	6.61	100
Temporal pole (STG)	R	40	10	−28	38	4.04	27
Parahippocampal gyrus	R	26	−26	−20	35	5.92	111
Parahippocampal gyrus	R	18	−38	−4	30	5.12	25
Parahippocampal gyrus	L	−28	−44	−6	19, 37	4.08	48
Lingual gyrus	R	6	−92	−10	17	4.28	21
Globus pallidus	R	16	−10	−2		4.12	21

Coordinates and *t* value refer to the peak of each brain region. MNI, Montreal Neurological Institute; BA, Brodmann area; L, left; R, right; MTG, middle temporal gyrus; STG, superior temporal gyrus BRM, basketball-related motions; BOM, basketball-unrelated motions; EBA, extrastriate body area; STS, superior temporal sulcus. All values, $P < .001$, uncorrected. *$P < .05$, corrected for multiple comparisons across a small volume of interest.

corrected for multiple comparisons across a small VOI. No significantly greater activation was identified in patients in the group comparison of the BRM minus BUM contrast.

Regression analysis revealed negative linear correlations between the negative scale score of PANSS and the degree of activation in the left EBA ($x = -58$, $y = -58$, $z = -6$; $t = 7.01$) in BRM minus BUM contrast (figure 3). Scores of the general psychopathology scale were also negatively correlated with the degree of activation in the left EBA ($x = -58$, $y = -56$, $z = -6$; $t = 5.81$) (figure 3). These correlations in a priori regions (EBA) survived a threshold of $P < .05$ corrected for multiple comparisons across a small VOI. There was no correlation between the positive scale score and regional brain activation. Regression analysis revealed that none of age, duration of illness, or chlorpromazine equivalent daily dosage had a relation with regional brain activation.

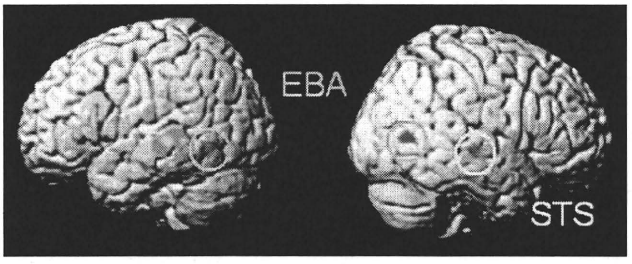

Fig. 2. Images Showing the Brain Area of Diminished Activations in Response to Basketball-Related Motions (BRM) Relative to Basketball-Unrelated Motions (BUM) Condition in 12 Patients With Schizophrenia Compared With 12 Normal Controls. Diminished activations in the bilateral extrastriate body area (EBA), right superior temporal sulcus (STS), and right temporal pole are shown.

Discussion

This study demonstrated that patients with schizophrenia showed diminished brain activations during observation of context-congruent actions in the EBA, along with the STS. The coordinates of the EBA were in good agreement with the previous literature (reviewed in Arzy et al[29]). The lesser activation of the STS in the patients was fairly predicted because previous psychological study has shown the impairment of biological motion perception in schizophrenia, which has been thought to be attributable to dysfunction of the STS.[18] The STS is located at a convergence zone for multimodal signals including limbic information,[30] and it has been suggested to be involved not only in the perception of biological motion but also in a more extended function of social cognition such as understating others' intention.[16,17] Dysfunctional STS might contribute to a difficulty in understanding intentional actions and behavior of agents in schizophrenia.[31]

The novel finding in this study was that the patients showed diminished EBA activation in response to context-congruent actions despite the fact that the patients comprehended explicit information of body movement (and basketball rules) similar to controls. This implies that the patients might not have processed implicit information carried by body movements as much as controls, but it is very difficult to quantify such implicit information and complex EBA function in a limited MRI environment and in a limited time period. Interestingly, PANSS score, instead of performance during fMRI scans, was directly linked to EBA activation in patients. That is, the less EBA activation was, the more severe the symptoms (negative and general psychopathology) in the patients were. The EBA was first identified as an area that responds selectively to static human bodies.[19] Recent

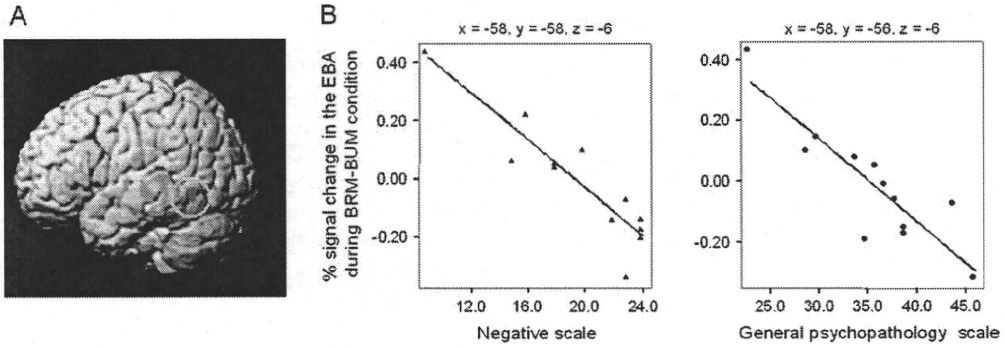

Fig. 3. Negative Correlations Between Positive and Negative Syndrome Scale (PANSS) Scores and the Degree of Activation in the Extrastriate Body area (EBA). A, Images showing negative correlation between negative scale scores and the degree of activation in the left EBA in basketball-related motions-basketball-unrelated motions (BRM-BUM) contrast. Scores of general psychopathology scale were also negatively correlated with the degree of activation in the left EBA in BRM-BUM contrast, yielding images identical to A. B, Plots and regression lines of negative correlations between PANSS scores and the degree of activation in the left EBA. The degrees of activations in the EBA were negatively correlated with the scores of negative scale ($r = -0.91$, $df = 10$; $P < .001$) and general psychopathology scale ($r = -0.88$, $df = 10$; $P < .001$).

studies have suggested that the EBA is also directly involved in representing the dynamic aspects of human motions as part of a system for inferring the intention of others.[32] Jackson et al[22] reported that, compared with observation of actions, EBA activation was enhanced during imitation. Furthermore, the motivation to act has been shown to modulate EBA activity.[33] These studies proposed an extended role for the EBA, involving the planning, execution, and imagination of actions. Our previous report that using the current task in healthy volunteers was in favor of this view,[23] suggesting that the EBA might contribute to the understanding of actions and intention of others through the mechanism of observed action being automatically represented and simulated.[14,32]

Empirical studies have shown that schizophrenia patients have difficulty in representing motor actions internally.[34,35] The diminished EBA activation in patients suggests that internal representation of the dynamic aspects of human motions is impaired. Motor representation is associated with understanding and rehearsing observed behavior.[14] In fact, recent studies demonstrated that motor representation is highly involved in skill learning and motor rehabilitation.[36,37] Consequently, the deficit in the EBA in schizophrenia could lead to difficulties in learning and reproducing new skills in addition to impairment in understanding others' actions.

The present study has several limitations. First, we examined only patients with chronic schizophrenia with long-term antipsychotic medication because our primary interest was the possible role of sports participation/observation in the management of chronic schizophrenia and comorbid metabolic disturbances partly due to antipsychotic medication. Medication possibly affects neural activation, but regression analysis revealed that chlorpromazine equivalent daily dosage has no relation with regional brain activation, and expression of dopamine D2 receptors in the posterior temporal-occipital cortex is extremely low.[38] Second, our task was not a behaviorally/cognitively demanding task leading to lack of dispersion in behavioral data (100% accuracy for both control and patient groups). Using a behaviorally/cognitively demanding task would require us to include only patients with psychiatric symptoms and cognitive impairments mild enough to undergo the imaging procedure and comply with the demanding task. However, the target patients of rehabilitation and management of comorbid metabolic disturbances in a day hospital have considerable behavioral and cognitive disturbances, which make it difficult to obtain reliable self-reported data of complex and subtle functions. Therefore, we employed the current task, aiming to examine patients with chronic schizophrenia in a real-world setting. From these limitations, it must be emphasized that any generalization of our findings to patients with first episode or nondeficit patients needs to be approached with caution.

In conclusion, chronic schizophrenia patients demonstrated diminished activation in the EBA in response to sports-related actions. Dysfunction of the EBA might reflect impairment of representation of dynamic aspects of human actions and might lead to impairments in simulation, learning, and execution of actions in schizophrenia. Furthermore, these impairments might lead to difficulty in understanding others' actions, interpersonal communication, body awareness, and overall physical activity manifested as negative symptoms and general psychopathology symptoms. The results of this study seem to have some important clinical implications for the management of chronic schizophrenia and merit further investigation in terms of the role of sports participation/observation in the rehabilitation for chronic schizophrenia and their effects on EBA function.

Funding

Japanese Ministry of Health, Labor and Welfare (Health and Labor Sciences Research Grant for Research on

Psychiatric and Neurological Diseases and Mental Health H20-KOKORO-025).

Acknowledgments

Mieko Mori and Harumi Murayama and the staff of the day hospital unit of Asai Hospital are gratefully acknowledged for nursing care and assistance with subject recruitment.

References

1. Henderson DC. Diabetes mellitus and other metabolic disturbances induced by atypical antipsychotic agents. *Curr Diab Rep*. 2002;2:135–140.
2. Menza M, Vreeland B, Minsky S, Gara M, Radler DR, Sakowitz M. Managing atypical antipsychotic-associated weight gain: 12-month data on a multimodal weight control program. *J Clin Psychiatry*. 2004;65:471–477.
3. Langle G, Siemssen G, Hornberger S. Role of sports in treatment and rehabilitation of schizophrenic patients. *Rehabilitation (Stuttg)*. 2000;39:276–282.
4. Daumit GL, Goldberg RW, Anthony C, et al. Physical activity patterns in adults with severe mental illness. *J Nerv Ment Dis*. 2005;193:641–646.
5. Faulkner G, Cohn T, Remington G. Validation of a physical activity assessment tool for individuals with schizophrenia. *Schizophr Res*. 2006;82:225–231.
6. Boks MP, Russo S, Knegtering R, van den Bosch RJ. The specificity of neurological signs in schizophrenia: a review. *Schizophr Res*. 2000;43:109–116.
7. Kodama S, Fukuzako H, Fukuzako T, et al. Aberrant brain activation following motor skill learning in schizophrenic patients as shown by functional magnetic resonance imaging. *Psychol Med*. 2001;31:1079–1088.
8. Weickert TW, Terrazas A, Bigelow LB, et al. Habit and skill learning in schizophrenia: evidence of normal striatal processing with abnormal cortical input. *Learn Mem*. 2002;9:430–442.
9. Alexander GE, DeLong MR, Strick PL. Parallel organization of functionally segregated circuits linking basal ganglia and cortex. *Annu Rev Neurosci*. 1986;9:357–381.
10. Andreasen NC. A unitary model of schizophrenia: Bleuler's "fragmented phrene" as schizencephaly. *Arch Gen Psychiatry*. 1999;56:781–787.
11. Grezes J, Decety J. Functional anatomy of execution, mental simulation, observation, and verb generation of actions: a meta-analysis. *Hum Brain Mapp*. 2001;12:1–19.
12. Iacoboni M, Dapretto M. The mirror neuron system and the consequences of its dysfunction. *Nat Rev Neurosci*. 2006; 7:942–951.
13. Chartrand TL, Bargh JA. The chameleon effect: the perception-behavior link and social interaction. *J Pers Soc Psychol*. 1999;76:893–910.
14. Brass M, Heyes C. Imitation: is cognitive neuroscience solving the correspondence problem? *Trends Cogn Sci*. 2005; 9:489–495.
15. Allison T, Puce A, McCarthy G. Social perception from visual cues: role of the STS region. *Trends Cogn Sci*. 2000;4:267–278.
16. Frith U, Frith CD. Development and neurophysiology of mentalizing. *Philos Trans R Soc Lond B Biol Sci*. 2003;358:459–473.
17. Gallagher HL, Frith CD. Functional imaging of 'theory of mind'. *Trends Cogn Sci*. 2003;7:77–83.
18. Kim J, Doop ML, Blake R, Park S. Impaired visual recognition of biological motion in schizophrenia. *Schizophr Res*. 2005;77:299–307.
19. Downing PE, Jiang Y, Shuman M, Kanwisher N. A cortical area selective for visual processing of the human body. *Science*. 2001;293:2470–2473.
20. Peelen MV, Wiggett AJ, Downing PE. Patterns of fMRI activity dissociate overlapping functional brain areas that respond to biological motion. *Neuron*. 2006;49:815–822.
21. Astafiev SV, Stanley CM, Shulman GL, Corbetta M. Extrastriate body area in human occipital cortex responds to the performance of motor actions. *Nat Neurosci*. 2004;7:542–548.
22. Jackson PL, Meltzoff AN, Decety J. Neural circuits involved in imitation and perspective-taking. *Neuroimage*. 2006;31:429–439.
23. Takahashi H, Shibuya T, Kato M, et al. Enhanced activation in the extrastriate body area by goal-directed actions. *Psychiatry Clin Neurosci*. 2008;62:214–219.
24. Torrey EF. Schizophrenia and the inferior parietal lobule. *Schizophr Res*. 2007;97:215–225.
25. Rey MJ, Schulz P, Costa C, Dick P, Tissot R. Guidelines for the dosage of neuroleptics. I: Chlorpromazine equivalents of orally administered neuroleptics. *Int Clin Psychopharmacol*. 1989;4:95–104.
26. Rijcken CA, Monster TB, Brouwers JR, de Jong-van den Berg LT. Chlorpromazine equivalents versus defined daily doses: how to compare antipsychotic drug doses? *J Clin Psychopharmacol*. 2003;23:657–659.
27. Kay SR, Fiszbein A, Opler LA. The positive and negative syndrome scale (PANSS) for schizophrenia. *Schizophr Bull*. 1987;13:261–276.
28. Maldjian JA, Laurienti PJ, Kraft RA, Burdette JH. An automated method for neuroanatomic and cytoarchitectonic atlas-based interrogation of fMRI data sets. *Neuroimage*. 2003; 19:1233–1239.
29. Arzy S, Thut G, Mohr C, Michel CM, Blanke O. Neural basis of embodiment: distinct contributions of temporoparietal junction and extrastriate body area. *J Neurosci*. 2006;26:8074–8081.
30. Puce A, Perrett D. Electrophysiology and brain imaging of biological motion. *Philos Trans R Soc Lond B Biol Sci*. 2003; 358:435–445.
31. Russell TA, Reynaud E, Herba C, Morris R, Corcoran R. Do you see what I see? Interpretations of intentional movement in schizophrenia. *Schizophr Res*. 2006;81:101–111.
32. Jeannerod M. Visual and action cues contribute to the self-other distinction. *Nat Neurosci*. 2004;7:422–423.
33. Cheng Y, Meltzoff AN, Decety J. Motivation modulates the activity of the human mirror-neuron system. *Cereb Cortex*. 2007;17:1979–1986.
34. Danckert J, Rossetti Y, d'Amato T, Dalery J, Saoud M. Exploring imagined movements in patients with schizophrenia. *Neuroreport*. 2002;13:605–609.
35. Maruff P, Wilson P, Currie J. Abnormalities of motor imagery associated with somatic passivity phenomena in schizophrenia. *Schizophr Res*. 2003;60:229–238.
36. Calvo-Merino B, Glaser DE, Grezes J, Passingham RE, Haggard P. Action observation and acquired motor skills: an FMRI study with expert dancers. *Cereb Cortex*. 2005;15:1243–1249.
37. Ertelt D, Small S, Solodkin A, et al. Action observation has a positive impact on rehabilitation of motor deficits after stroke. *Neuroimage*. 2007;36(Suppl. 2):T164–173.
38. Okubo Y, Olsson H, Ito H, et al. PET mapping of extrastriatal D2-like dopamine receptors in the human brain using an anatomic standardization technique and [11C]FLB 457. *Neuroimage*. 1999;10:666–674.

NeuroImage 49 (2010) 121–126

Contents lists available at ScienceDirect

NeuroImage

journal homepage: www.elsevier.com/locate/ynimg

Reduced serotonin transporter binding in the insular cortex in patients with obsessive–compulsive disorder: A [^{11}C]DASB PET study

Ryohei Matsumoto [a,b], Masanori Ichise [a,c], Hiroshi Ito [a], Tomomichi Ando [a,d], Hidehiko Takahashi [a], Yoko Ikoma [a], Jun Kosaka [a], Ryosuke Arakawa [a], Yota Fujimura [a,e], Miho Ota [a], Akihiro Takano [a], Kenji Fukui [b], Kazuhiko Nakayama [d], Tetsuya Suhara [a,*]

[a] *Molecular Neuroimaging Group, Molecular Imaging Center, National Institute of Radiological Sciences, 4-9-1, Anagawa, Inage-ku, Chiba, 263-8555, Japan*
[b] *Department of Psychiatry, Graduate School of Kyoto Prefectural University of Medicine, Kyoto, Japan*
[c] *Department of Radiology, Columbia University, New York, USA*
[d] *Department of Psychiatry, Jikei University School of Medicine, Tokyo, Japan*
[e] *Department of Psychiatry, School of Medicine, Teikyo University, Tokyo, Japan*

ARTICLE INFO

Article history:
Received 15 April 2009
Revised 25 July 2009
Accepted 29 July 2009
Available online 4 August 2009

Keywords:
Obsessive–compulsive disorder (OCD)
Positron emission tomography (PET)
Serotonin transporter
Insular cortex
Voxel based analysis

ABSTRACT

The serotonin transporter (5-HTT) and other markers of the serotonergic system have been of interest in the pathophysiology of obsessive-compulsive disorder (OCD). Previous studies using single photon emission computed tomography (SPECT) with [^{123}I]β-CIT or positron emission tomography (PET) with [^{11}C]McN5652 have not shown consistent findings about 5-HTT in OCD patients. The aim of the present study was to investigate 5-HTT binding using [^{11}C]DASB, which has higher selectivity or specific binding-to-nonspecific binding ratios for 5-HTT compared to the aforementioned radioligands. Four drug-naive and 6 drug-free patients with OCD who were free of comorbid depression and 18 gender and age-matched healthy subjects underwent PET scans with [^{11}C]DASB. The severity of OCD was assessed by Yale–Brown Obsessive–Compulsive Scale (Y-BOCS) (mean ± SD: 22 ± 7.6, range: 7–32). The binding potential (BP_{ND}) of [^{11}C]DASB was calculated using a two-parameter multilinear reference tissue model (MRTM2). The parametric images of BP_{ND} were analyzed using a statistical parametric mapping system. Significant reductions of BP_{ND} were observed in the right posterior and left anterior insular cortices in patients with OCD compared to controls. Region-of-interest analysis has also confirmed significant reduction of BP_{ND} in the insular cortex. Although significantly reduced BP_{ND} in the orbitofrontal cortex was also observed in patients with OCD compared to controls, this finding should be considered with caution because of the very low 5-HTT binding in the region. On the other hand, no significant correlation was observed between the Y-BOCS score and BP_{ND}. The change in [^{11}C]DASB binding in the insular cortex suggests that dysfunction of the serotonergic system in the limbic area might be involved in the pathophysiology of OCD.

Introduction

Obsessive–compulsive disorder (OCD) is a common chronic psychiatric disorder characterized by recurrent obsessions and compulsions. OCD has a high lifetime prevalence rate of 2–3% in the general population and is considered to be among the twenty leading causes of disability in the United States and other countries (Michaud et al., 2006). Based on a number of pertinent findings, such as the effect of serotonin reuptake inhibitors (SSRIs), high comorbidity of depression, reduced densities of platelet serotonin transporter (5-HTT), and the association of 5-HTT gene polymorphism in OCD (Greist and Jefferson, 1998; Greist et al., 1995; Lin, 2007; March, 1997), the serotonergic system including 5-HTT has attracted considerable attention in relation to the pathophysiology of OCD.

5-HTT in living human brain can be measured by positron emission tomography (PET) and single photon emission computed tomography (SPECT) with several radioligands. Inconsistent findings in [^{123}I]β-CIT binding in the thalamus and midbrain of patients with OCD were reported by SPECT studies (Hesse et al., 2005; Pogarell et al., 2003; Simpson et al., 2003; Stengler-Wenzke et al., 2004; Zitterl et al., 2007). Since [^{123}I]β-CIT also has affinity to dopamine transporter, it is not an ideal radioligand for quantifying 5-HTT. In a prior PET study using [^{11}C]McN5652, a selective radioligand for 5-HTT, no significant differences were observed in patients with OCD compared to normal subjects (Simpson et al., 2003). However, [^{11}C]McN5652 shows relatively higher nonspecific binding and lower specific binding-to-nonspecific binding ratios compared to [^{11}C]DASB (Huang et al., 2002), a radioligand with higher specific binding to 5-HTT (Wilson et al., 2002) that allows the quantification of binding of not only 5-HTT-rich

* Corresponding author. Fax: +81 43 253 0396.
E-mail addresses: rmat.jpn@gmail.com (R. Matsumoto), suhara@nirs.go.jp (T. Suhara).

1053-8119/$ – see front matter © 2009 Elsevier Inc. All rights reserved.
doi:10.1016/j.neuroimage.2009.07.069

regions but also relatively low density regions such as cerebral cortices (Ichise et al., 2003; Kim et al., 2006). The aim of the present study was to investigate 5-HTT in the brain of patients with OCD using [^{11}C]DASB.

Materials and methods

Subjects

Ten patients with OCD and 18 healthy control subjects participated in this study. All patients met DSM-IV criteria for OCD. Clinical diagnosis was completed by three trained psychiatrists. Based on conventional unstructured interviews and medical histories, we excluded patients with psychiatric disorders other than OCD, such as current major depressive disorder, schizophrenia, bipolar disorders, other anxiety disorders, and substance abuse. To rule out somatic disorders, all patients underwent physical, neurological, blood, and urine examinations. Demographic and clinical data of the patients are summarized in Table 1. Four patients were psychotropic-naive, and six patients had a history of SSRI or SRI treatment. They had not received medication for at least 5 weeks prior to the PET scans. Severity of symptoms was assessed using the Japanese version of the Yale–Brown Obsessive–Compulsive Scale (Y-BOCS) on the day of the PET scan (Goodman et al., 1989a,b; Nakajima et al., 1995). Most patients received cognitive-behavioral therapy and one subject showed significant improvement until the day of the PET scan.

Eighteen age- and gender-matched healthy control subjects, 7 males and 11 females with a mean age of 30 yr (range 20–47), were recruited from the surrounding community. Based on unstructured psychiatric screening interviews, they were free of current and past psychiatric or somatic disorders, and had no history of drug abuse.

Smokers among the participants were 3 and 1 in the OCD patients and controls, respectively.

After providing a complete explanation of the study, written informed consent was obtained from all subjects. This study was approved by the Ethics and Radiation Safety Committee of the National Institute of Radiological Sciences, Chiba, Japan.

PET procedures

[^{11}C]DASB was synthesized by methylation of the corresponding des-methyl precursor with [^{11}C]CH_3I (Wilson et al., 2000a,b). Radiochemical purity was >95%.

A 10-min transmission scan was done to correct for attenuation. Dynamic PET scans were carried out for 90 min (1 min × 4, 2 min × 13, 4 min × 5, 8 min × 5) in 2D mode immediately after a bolus injection of 692–967 MBq (mean ± SD: 725 ± 71 MBq) of [^{11}C]DASB with high specific radioactivities (116–194 GBq/μmol; mean ± SD, 154 ± 44 GBq/μmol) at the time of injection. A head fixation device of thermoplastic attachments for individual fit with minimized head movement was used during the PET scans.

PET scans were performed for 5 of the 10 patients using a Siemens ECAT47 system (Siemens, Knoxville, TN), which provides 47 slices and a 16.2 cm field-of-view, and the data were reconstructed with a Ramp filter with a cut-off frequency of 0.5 (full-width half maximum [FWHM], 6.3 mm). The other 5 patients were measured by EXACT HR + scanner, which provides 63 planes and a 15.5 cm field-of-view, and the data were reconstructed with a Hanning filter with a cut-off frequency of 0.5 (FWHM 7.5 mm).

Similarly, PET scans were performed for 9 of the 18 healthy subjects using the Siemens ECAT47 system and for the other 9 healthy subjects using the EXACT HR+ system. Although two different PET cameras were used in this study, the scan protocol and controls were matched.

MRI procedures

T1-weighted magnetic resonance (MR) images were acquired using Philips Intera, 1.5 tesla (Philips Medical Systems, Best, The Netherlands). The scan parameters were 1 mm thick, 3D, T1 images with a transverse plane (repetition time [TR] / echo time [TE] = 19 / 10 ms, flip angle 30°, matrix 256 × 256, field-of-view [FOV] 256 mm × 256 mm).

Image analysis

Preprocessing

The original reconstructed PET data were corrected for head motion by aligning all frames to a mean image of all frames using Statistical Parametric Mapping 2 (SPM2; Wellcome Department of Cognitive Neurology, London, England) (Friston et al., 1995). The realigned PET image frames were then coregistered to individual MR images using SPM2. The coregistered PET data were transformed to the custom MRI template space using the transformation parameters from the individual MRI to the custom template MRI. In the present study, a custom MRI template was created from all subjects (Good et al., 2001). Then, each image was normalized anatomically and averaged into the custom MRI template.

Several regions of interest (ROIs) were manually defined on the custom MRI template, and time–activity curves of each ROI of the cerebellum, midbrain, caudate, putamen, thalamus, prefrontal cortex, orbitofrontal cortex, parietal cortex, insular cortex, and cingulate cortex were obtained.

Model analysis

The binding potential (BP_{ND}) (Innis et al., 2007) was calculated using a two-parameter multilinear reference tissue model (MRTM2) (Ichise et al., 2003). MRTM2 was expressed by

$$C(T) = R_1 k'_2 \int_0^T C'(t)dt - k_2 \int_0^T C(t)dt + R_1 C'(T)$$

where $C(t)$ and $C'(t)$ are the regional or voxel time-radioactivity concentrations, k_2 and k_2' are the tracer clearance rates from tissue

Table 1
Clinical characteristics of subjects with obsessive–compulsive disorder.

No	Gender	Age (yr)	Duration of illness (yr)	Y-BOCS	Prior treatment	
					Pretreatment with SRIs	CBT
1	M	31	7	20	Free	+
2	F	35	14	24	Free	+
3	M	24	10	7	Free	+
4	F	24	3	18	Naive	−
5	M	21	2	29	Free	−
6	M	22	10	21	Naive	+
7	F	46	22	29	Free	+
8	F	28	1	18	Naive	+
9	F	38	26	32	Free	+
10	F	23	9	20	Naive	+
Total	4M/6F	21–46 (30 ± 8.4)	10.4 ± 8.8	7–32 (22 ± 7.6)	4 naive and 6 drug-free (>5 weeks)	8 treated/2 untreated

Data are shown as mean ± SD. cognitive-behavioral therapy (CBT), serotonin transporter reuptake inhibitors (SRIs).

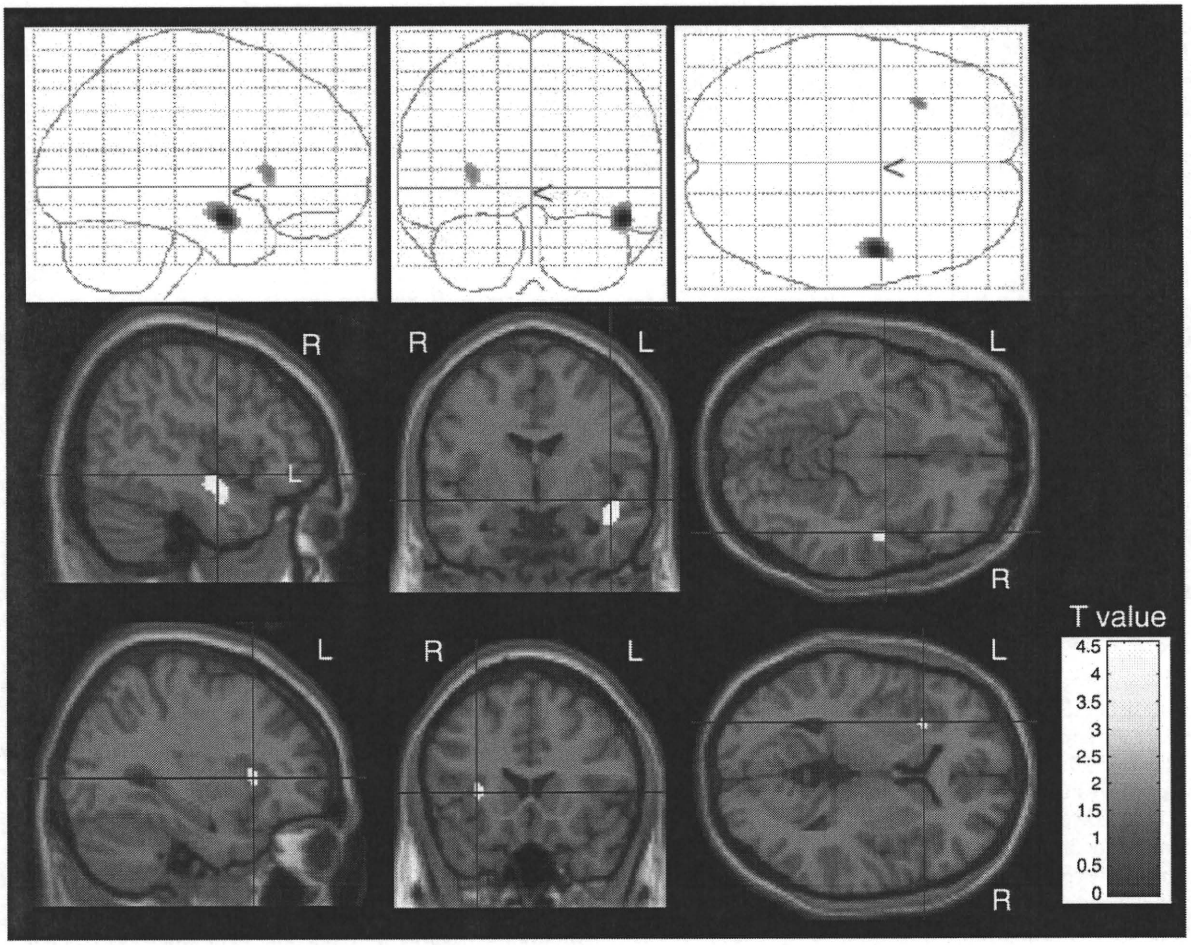

Fig. 1. Areas of reduced [^{11}C]DASB binding potential (BP_{ND}) in patients with OCD relative to healthy controls. SPM2 projections superimposed on representative transaxial, sagittal, and coronal magnetic resonance images (threshold for display: $p<0.001$, uncorrected with 25 or more contiguous voxels; voxel size = 2*2*2 mm, masked out by the absolute threshold of $BP_{ND}>0.15$).

that become constant for $T>t^*$, R_1 is the relative tracer delivery (K_1 / K_1'), and the prime sign indicates the reference region. MRTM2 provides relatively lower variability and bias of [^{11}C]DASB BP_{ND} compared to other model analyses without arterial data (Ichise et al., 2003). MRTM2 allows the estimation of $BP_{ND} = f_{ND}B_{max} / K_D$, which is proportional to the transporter density (B_{max}), where f_{ND} and K_D are the free fraction of the ligand in the nondisplaceable tissue compartment and dissociation constant, respectively. The cerebellum was used as the reference tissue because of its negligible density of 5-HTT (Kish et al., 2005). The cerebellar time–activity curves normalized by injected radioactivity were almost equal between the patients and control subjects in the present study (data not shown). In a previous study, the k_2' value was estimated by the three-parameter multilinear reference tissue model (MRTM) using the tissue time–activity curve (Ichise et al., 2002). To minimize the variability of k_2' estimation by MRTM, a weighted (according to ROI size) mean k_2' value over the midbrain, thalamus, and striatum calculated with the cerebellum as reference region was used for estimating BP_{ND} by MRTM2. This method achieved 4–8% of BP_{ND} variability in the frontal cortex, midbrain, thalamus, and striatum in the test–retest study for [^{11}C] DASB (Kim et al., 2006). All BP_{ND} estimations were performed with Pmod 2.65 (PMOD Technologies, Ltd., Zurich, Switzerland).

Parametric imaging analysis

Using the weighted mean k_2' value mentioned above, parametric images of BP_{ND} were generated by MRTM2. These images were smoothed with a Gaussian filter to 12-mm FWHM. Comparisons of BP_{ND} between the OCD group and control group were performed voxel-wise using SPM2, and the absolute threshold of BP_{ND} was set at 0.15. The statistical threshold was set at $p<0.001$, uncorrected for multiple comparisons ($T=3.50$) and 25 or more contiguous voxels.

Table 2
Regional [^{11}C]DASB binding potential (BP_{ND}) values in control subjects and subjects with obsessive–compulsive disorder (OCD).

Regions	[^{11}C]DASB BP_{ND} Values (Mean ± SD)		% difference[a]	p-value[b]
	Control subjects ($n=18$)	OCD subjects ($n=10$)		
Caudate	0.94 ± 0.25	0.82 ± 0.04	−12%	0.08
Putamen	1.20 ± 0.25	1.13 ± 0.06	−6.3%	0.23
Thalamus	1.46 ± 0.37	1.31 ± 0.12	−10%	0.14
Midbrain	2.99 ± 0.82	2.53 ± 0.46	−15%	0.06
Prefrontal cortex	0.19 ± 0.06	0.14 ± 0.03	−26%	0.008
Orbitofrontal cortex	0.13 ± 0.05	0.08 ± 0.02	−42%	0.0005**
Temporal cortex	0.43 ± 0.12	0.34 ± 0.03	−20%	0.007
Parietal cortex	0.13 ± 0.06	0.10 ± 0.03	−17%	0.12
Insular cortex	0.43 ± 0.11	0.30 ± 0.04	−30%	0.0008**
Cingulate cortex	0.38 ± 0.10	0.31 ± 0.04	−18%	0.01

Subjects with OCD showed significantly lower [^{11}C]DASB BP_{ND} in the orbitofrontal cortex and insular cortex compared to control subjects.

[a] % difference: (mean BP_{ND} of OCD subjects − mean BP_{ND} of control subjects) / mean BP_{ND} of control subjects × 100.

[b] Welch's t statistics was performed using Bonferroni's correction for each set of 10 regional measures, and the level of significant was set as follows: *$p<0.005 = 0.05 / 10$, **$p<0.001 = 0.01 / 10$.

Within the OCD group, correlation between regional BP_{ND} parametric images and OC symptom severity measured using Y-BOCS was evaluated by SPM2. The age of patients with OCD was entered as confounding factor in the analysis of covariance. The threshold was set at $p<0.001$, uncorrected for multiple comparisons ($T=3.50$) and 25 or more contiguous voxels.

ROI analysis

Using the weighted mean k_2' value, the BP_{ND} values in the 10 ROIs mentioned above were calculated by MRTM2. Group differences in BP_{ND} values of regions between patients and control subjects were compared using Welch's t statistics with Bonferroni's correction for multiple comparisons. All statistical tests were two-sided, and significance was defined as $p<0.005=0.05/10$. Further, the % differences between groups were calculated as follows: (mean BP_{ND} of OCD subjects − mean BP_{ND} of control subjects) / mean BP_{ND} of control subjects × 100.

Within the OCD group, correlational analysis between BP_{ND} of each ROI and Y-BOCS score was done using age as a covariate, and significance was defined as two-sided $p<0.005=0.05/10$.

Results

SPM analysis of BP_{ND} parametric images revealed significant reductions in the right posterior and left anterior insular cortex in the patients with OCD compared to healthy controls (Fig. 1).

ROI analysis revealed that the BP_{ND} values of the OCD patients had a tendency to be lower compared to control subjects in all regions (Table 2). Among them, the BP_{ND} values showed significant reductions compared to healthy controls in the insular cortex ($p=0.0008<0.001$) and orbitofrontal cortex ($p=0.0005<0.001$) (Table 2 and Fig. 2), and were 30% and 42% lower than those of healthy controls, respectively. These % differences were apparently larger than those of the other regions, especially 5-HTT-rich regions including the thalamus, striatum, and midbrain. Using a lower statistical threshold ($p<0.01$, uncorrected), there was no trend of group differences in 5-HTT-rich regions such as the midbrain, thalamus, and striatum. In particular, although we performed additional SPM analysis with a cluster size>0 voxel, there were no significant BP differences in the midbrain including the raphe nucleus.

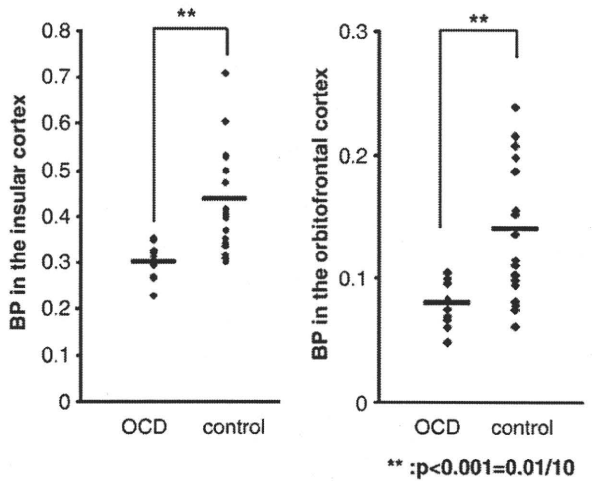

Fig. 2. Scatter plot of [^{11}C]DASB binding potential (BP_{ND}) in the insular cortex and orbitofrontal cortex. Region-of-interest (ROI) analysis revealed significant group differences in the BP_{ND} values of the insular cortex and orbitofrontal cortex within the 10 regions. Statistics were performed using Welch's t statistics with Bonferroni's correction for multiple comparisons.

Table 3
Relationships between regional [^{11}C]DASB binding potential (BP_{ND}) values and Y-BOCS score in subjects with obsessive–compulsive disorder (OCD).

Regions	*p* value	*r* value
Caudate	0.10	0.34
Putamen	0.15	0.27
Thalamus	0.20	0.11
Midbrain	0.56	0.05
Prefrontal cortex	0.44	0.08
Orbitofrontal cortex	0.98	0.0001
Temporal cortex	0.18	0.27
Parietal cortex	0.19	0.23
Insular cortex	0.76	0.01
Cingulate cortex	0.06	0.41

Correlational analysis between regional [^{11}C]DASB BP_{ND} Values and Y-BOCS Score was performed using age as a covariate. Statistical threshold was set at two-side $p<0.005=0.05/10$.

There were no significant correlations or trends between Y-BOCS score and BP_{ND} in any of the brain regions by either SPM or ROI analysis. The correlation coefficient and *p*-value in each region as clarified by ROI analysis are described in Table 3.

Discussion

In the present study, significantly lower BP_{ND} values in the insular cortex were observed by [^{11}C]DASB PET study in OCD patients free of comorbid depression, compared to healthy controls. Especially, voxel-based analysis of parametric images over the whole brain contributed to the above new finding. Intriguingly, the [^{11}C]DASB BP_{ND} values in the orbitofrontal cortex also showed a significant reduction in OCD patients compared to healthy controls. The orbitofrontal cortex is one of the regions suggested to be strongly involved in the pathophysiology of OCD (Menzies et al., 2008). However, the BP_{ND} values in the orbitofrontal cortex were very low in the whole brain (Table 2 and Fig. 2). Considering the accuracy of the PET data, this finding should be considered with caution. In addition, there were no significant volume differences in the insular cortex and orbitofrontal cortex between the groups (data not shown) using the voxel-based morphometric approach (Good et al., 2001).

No significant differences in BP_{ND} were observed in 5-HTT-rich regions such as the midbrain, thalamus, and striatum by both SPM and ROI analyses in the present study. The absence of significant changes in BP_{ND} of [^{11}C]DASB in 5-HTT-rich regions was consistent with the previous [^{11}C]McN5652 PET study (Simpson et al., 2003) and [^{123}I]β-CIT SPECT study (van der Wee et al., 2004). On the other hand, reduced 5-HTT binding was reported by [^{123}I]β-CIT SPECT studies in the midbrain (Stengler-Wenzke et al., 2004) and thalamus (Zitterl et al., 2007). A recent report by Reimold et al. showed reduced 5-HTT binding in the thalamus and midbrain in 9 drug-free patients with OCD using ROI analysis of [^{11}C]DASB PET (Reimold et al., 2007). In addition, increased 5-HTT binding in the midbrain was shown in another [^{123}I]β-CIT SPECT study (Pogarell et al., 2003). These inconsistencies may be partially due to the differences in radioligand. Another explanation might be the heterogeneity of the subjects, as OCD is clinically heterogeneous, and different OC symptom dimensions may be involved in different neural components (Mataix-Cols et al., 2005, 2004). Furthermore, a relatively small sample size, a limitation of both the study by Reimold et al. and the present study, may have caused the inconsistencies. Thus, further studies will be required to establish whether 5-HTT bindings in 5-HTT-rich regions are altered or not in patients with OCD.

The insular cortex is part of the paralimbic circuit encompassing orbitofrontal and cingulate cortices and is thought to play an important role in emotional processing (Phillips et al., 1997; Stark et al., 2003). Several neuroimaging studies have revealed that the insular cortex is activated when patients with OCD are confronted

with disgust-inducing stimuli (Phillips et al., 2000; Shapira et al., 2003; Stein et al., 2006, 2001). Functional neuroimaging studies have indicated that the administration of SSRIs modulates the neuronal responses of insula (Anderson et al., 2007; Arce et al., 2008; Nemoto et al., 2003). Thus, the present finding suggests that dysfunction of serotonergic neurotransmission in the insular cortex might underlie the pathophysiology of OCD.

The anti-OCD effect of SSRIs requires longer delay to obtain optimal therapeutic efficacy compared to depression (Blier and de Montigny, 1998). In contrast to depressive patients, depletion of serotonin in recovered OCD patients does not lead to a relapse (Berney et al., 2006). In rodents and pigs, chronic administration of SSRIs induces the desensitization of autoreceptors on terminals and the increase of 5-HT release in the orbitofrontal cortex, but not in the caudate (el Mansari and Blier, 1997, 2006). On the other hand, post-synaptic 5-HT receptors such as 5-HT2A and 2C receptors are not altered (El Mansari and Blier, 2005, 2006). Thus, chronic administration of SSRIs may exert their anti-OCD effect by enhancing the 5-HT transmission based on 5-HT autoreceptor adaptation (Blier and de Montigny, 1998; El Mansari and Blier, 2006). Actually, Adams et al. reported that increased 5-HT2A receptor binding in the caudate nuclei was detected in OCD patients using PET and altanserin (Adams et al., 2005). Although the desensitization of autoreceptors on 5-HT terminals in the insular cortex was not investigated, the revelation of such alterations of 5-HT transmission can be expected in this region in future studies.

In this study, there was no significant correlation between OCD severity and BP_{ND} in patients with OCD. The present finding regarding 5-HTT binding might be a trait of OCD irrespective of severity. Some of the previous studies also did not find a significant correlation between OCD severity and 5-HTT binding (Pogarell et al., 2003; Simpson et al., 2003; Stengler-Wenzke et al., 2004), whereas a negative correlation between reported in the thalamus (Reimold et al., 2007) and thalamus-hypothalamus (Zitterl et al., 2007). The clarification of whether 5-HTT binding is correlated with OCD severity will require the accumulation of additional findings.

There are several limitations in this study. Six patients had a history of SSRIs or SRIs treatment. Because chronic administration of SSRIs causes the down-regulation of 5-HTT (Benmansour et al., 1999; Horschitz et al., 2001), the effect of previous drug use could not be ruled out. To date, although the impact of psychotherapy on neurotransmission has not been revealed, possible confounding effects of cognitive-behavioral therapy on 5-HTT function cannot be ruled out. Investigation of the relationship between 5-HTT binding in patients with OCD and their heterogeneities in regard to age at onset, pretreatment with SRIs, and/or cognitive-behavioral therapy will be required. However, the limited sample size of the present study precluded any analysis of such relationships. In addition, rating scales for depressive symptoms or anxiety were not used in this study. Thus, the effect of sub-threshold depressive symptoms or anxiety on 5-HTT binding cannot be ruled out. Although it remains unclear whether smoking has an effect on 5-HTT binding in human brain, the inclusion of smokers in the present subjects with OCD and controls might be a possible confounding factor. Further, although two different PET cameras were used in this study, the scan protocol and controls were matched.

In conclusion, 5-HTT binding alteration in the insular cortex suggests that dysfunction of the serotonergic system in the insular cortex might be involved in the pathophysiology of OCD.

Acknowledgments

This study was supported by a Grant-in-Aid for the Molecular Imaging Program from the Ministry of Education, Culture, Sports, Science and Technology (MEXT), Japanese Government. We are grateful to all members of the cyclotron team at the National Institute of Radiological Sciences for their technical support in radioisotope production and all the radiological technicians for their help with the PET experiment. We also thank Ms. Yoshiko Fukushima for her help as clinical research coordinator.

References

Adams, K.H., Hansen, E.S., Pinborg, L.H., Hasselbalch, S.G., Svarer, C., Holm, S., Bolwig, T.G., Knudsen, G.M., 2005. Patients with obsessive–compulsive disorder have increased 5-HT2A receptor binding in the caudate nuclei. Int. J. Neuropsychopharmacol. 8, 391–401.

Anderson, I.M., Del-Ben, C.M., McKie, S., Richardson, P., Williams, S.R., Elliott, R., Deakin, J.F., 2007. Citalopram modulation of neuronal responses to aversive face emotions: a functional MRI study. Neuroreport 18, 1351–1355.

Arce, E., Simmons, A.N., Lovero, K.L., Stein, M.B., Paulus, M.P., 2008. Escitalopram effects on insula and amygdala BOLD activation during emotional processing. Psychopharmacology (Berl) 196, 661–672.

Benmansour, S., Cecchi, M., Morilak, D.A., Gerhardt, G.A., Javors, M.A., Gould, G.G., Frazer, A., 1999. Effects of chronic antidepressant treatments on serotonin transporter function, density, and mRNA level. J. Neurosci. 19, 10494–10501.

Berney, A., Sookman, D., Leyton, M., Young, S.N., Benkelfat, C., 2006. Lack of effects on core obsessive–compulsive symptoms of tryptophan depletion during symptom provocation in remitted obsessive–compulsive disorder patients. Biol. Psychiatry 59, 853–857.

Blier, P., de Montigny, C., 1998. Possible serotonergic mechanisms underlying the antidepressant and anti-obsessive–compulsive disorder responses. Biol. Psychiatry 44, 313–323.

el Mansari, M., Blier, P., 1997. In vivo electrophysiological characterization of 5-HT receptors in the guinea pig head of caudate nucleus and orbitofrontal cortex. Neuropharmacology 36, 577–588.

El Mansari, M., Blier, P., 2005. Responsiveness of 5-HT(1A) and 5-HT2 receptors in the rat orbitofrontal cortex after long-term serotonin reuptake inhibition. J. Psychiatry. Neurosci. 30, 268–274.

El Mansari, M., Blier, P., 2006. Mechanisms of action of current and potential pharmacotherapies of obsessive–compulsive disorder. Prog. Neuropsychopharmacol. Biol. Psychiatry 30, 362–373.

Friston, K.J., Holmes, A.P., Worseley, K.J., Poline, J.B., Frith, C.D., Frackowiack, R.S., 1995. Statistical parametric maps in functional imaging: a general linear approach. Human Brain Mapping 2, 189–210.

Good, C.D., Johnsrude, I.S., Ashburner, J., Henson, R.N., Friston, K.J., Frackowiak, R.S., 2001. A voxel-based morphometric study of ageing in 465 normal adult human brains. Neuroimage 14, 21–36.

Goodman, W.K., Price, L.H., Rasmussen, S.A., Mazure, C., Delgado, P., Heninger, G.R., Charney, D.S., 1989a. The Yale–Brown Obsessive–Compulsive Scale. II. Validity. Arch. Gen. Psychiatry 46, 1012–1016.

Goodman, W.K., Price, L.H., Rasmussen, S.A., Mazure, C., Fleischmann, R.L., Hill, C.L., Heninger, G.R., Charney, D.S., 1989b. The Yale–Brown Obsessive–Compulsive Scale. I. Development, use, and reliability. Arch. Gen. Psychiatry 46, 1006–1011.

Greist, J.H., Jefferson, J.W., 1998. Pharmacotherapy for obsessive–compulsive disorder. Br. J. Psychiatry. Suppl. 64–70.

Greist, J.H., Jefferson, J.W., Kobak, K.A., Katzelnick, D.J., Serlin, R.C., 1995. Efficacy and tolerability of serotonin transport inhibitors in obsessive–compulsive disorder. A meta-analysis. Arch. Gen. Psychiatry 52, 53–60.

Hesse, S., Muller, U., Lincke, T., Barthel, H., Villmann, T., Angermeyer, M.C., Sabri, O., Stengler-Wenzke, K., 2005. Serotonin and dopamine transporter imaging in patients with obsessive–compulsive disorder. Psychiatry Res. 140, 63–72.

Horschitz, S., Hummerich, R., Schloss, P., 2001. Down-regulation of the rat serotonin transporter upon exposure to a selective serotonin reuptake inhibitor. Neuroreport 12, 2181–2184.

Huang, Y., Hwang, D.R., Narendran, R., Sudo, Y., Chatterjee, R., Bae, S.A., Mawlawi, O., Kegeles, L.S., Wilson, A.A., Kung, H.F., Laruelle, M., 2002. Comparative evaluation in nonhuman primates of five PET radiotracers for imaging the serotonin transporters: [^{11}C]McN 5652, [^{11}C]ADAM, [^{11}C]DASB, [^{11}C]DAPA, and [^{11}C]AFM. J. Cereb. Blood Flow Metab. 22, 1377–1398.

Ichise, M., Liow, J.S., Lu, J.Q., Takano, A., Model, K., Toyama, H., Suhara, T., Suzuki, K., Innis, R.B., Carson, R.E., 2003. Linearized reference tissue parametric imaging methods: application to [^{11}C]DASB positron emission tomography studies of the serotonin transporter in human brain. J. Cereb. Blood Flow Metab. 23, 1096–1112.

Ichise, M., Toyama, H., Innis, R.B., Carson, R.E., 2002. Strategies to improve neuroreceptor parameter estimation by linear regression analysis. J. Cereb. Blood Flow Metab. 22, 1271–1281.

Innis, R.B., Cunningham, V.J., Delforge, J., Fujita, M., Gjedde, A., Gunn, R.N., Holden, J., Houle, S., Huang, S.C., Ichise, M., Iida, H., Ito, H., Kimura, Y., Koeppe, R.A., Knudsen, G.M., Knuuti, J., Lammertsma, A.A., Laruelle, M., Logan, J., Maguire, R.P., Mintun, M.A., Morris, E.D., Parsey, R., Price, J.C., Slifstein, M., Sossi, V., Suhara, T., Votaw, J.R., Wong, D.F., Carson, R.E., 2007. Consensus nomenclature for in vivo imaging of reversibly binding radioligands. J. Cereb. Blood Flow Metab. 27, 1533–1539.

Kim, J.S., Ichise, M., Sangare, J., Innis, R.B., 2006. PET imaging of serotonin transporters with [^{11}C]DASB: test–retest reproducibility using a multilinear reference tissue parametric imaging method. J. Nucl. Med. 47, 208–214.

Kish, S.J., Furukawa, Y., Chang, L.J., Tong, J., Ginovart, N., Wilson, A., Houle, S., Meyer, J.H., 2005. Regional distribution of serotonin transporter protein in postmortem human brain: is the cerebellum a SERT-free brain region? Nucl. Med. Biol. 32, 123–128.

Lin, P.Y., 2007. Meta-analysis of the association of serotonin transporter gene polymorphism with obsessive–compulsive disorder. Prog. Neuropsychopharmacol. Biol. Psychiatry 31, 683–689.

March, J.S., Frances, A., Kahn, D.A., Carpenter, D. (Eds.), 1997. The Expert Consensus Guideline Series: Treatment of Obsessive–Compulsive Disorder: J. Clin. Psychiatry, 58.

Mataix-Cols, D., Rosario-Campos, M.C., Leckman, J.F., 2005. A multidimensional model of obsessive–compulsive disorder. Am. J. Psychiatry 162, 228–238.

Mataix-Cols, D., Wooderson, S., Lawrence, N., Brammer, M.J., Speckens, A., Phillips, M.L., 2004. Distinct neural correlates of washing, checking, and hoarding symptom dimensions in obsessive–compulsive disorder. Arch. Gen. Psychiatry 61, 564–576.

Menzies, L., Chamberlain, S.R., Laird, A.R., Thelen, S.M., Sahakian, B.J., Bullmore, E.T., 2008. Integrating evidence from neuroimaging and neuropsychological studies of obsessive–compulsive disorder: the orbitofronto-striatal model revisited. Neurosci. Biobehav. Rev. 32, 525–549.

Michaud, C.M., McKenna, M.T., Begg, S., Tomijima, N., Majmudar, M., Bulzacchelli, M.T., Ebrahim, S., Ezzati, M., Salomon, J.A., Kreiser, J.G., Hogan, M., Murray, C.J., 2006. The burden of disease and injury in the United States 1996. Popul. Health. Metr. 4 (11).

Nakajima, T., Nakamura, M., Taga, C., Yamagami, S., Kiriike, N., Nagata, T., Saitoh, M., Kinoshita, T., Okajima, Y., Hanada, M., et al., 1995. Reliability and validity of the Japanese version of the Yale–Brown Obsessive–Compulsive Scale. Psychiatry Clin. Neurosci. 49, 121–126.

Nemoto, H., Toda, H., Nakajima, T., Hosokawa, S., Okada, Y., Yamamoto, K., Horiuchi, R., Endo, K., Ida, I., Mikuni, M., Goto, F., 2003. Fluvoxamine modulates pain sensation and affective processing of pain in human brain. Neuroreport 14, 791–797.

Phillips, M.L., Marks, I.M., Senior, C., Lythgoe, D., O'Dwyer, A.M., Meehan, O., Williams, S. C., Brammer, M.J., Bullmore, E.T., McGuire, P.K., 2000. A differential neural response in obsessive–compulsive disorder patients with washing compared with checking symptoms to disgust. Psychol. Med. 30, 1037–1050.

Phillips, M.L., Young, A.W., Senior, C., Brammer, M., Andrew, C., Calder, A.J., Bullmore, E.T., Perrett, D.I., Rowland, D., Williams, S.C., Gray, J.A., David, A.S., 1997. A specific neural substrate for perceiving facial expressions of disgust. Nature 389, 495–498.

Pogarell, O., Hamann, C., Popperl, G., Juckel, G., Chouker, M., Zaudig, M., Riedel, M., Moller, H.J., Hegerl, U., Tatsch, K., 2003. Elevated brain serotonin transporter availability in patients with obsessive–compulsive disorder. Biol. Psychiatry 54, 1406–1413.

Reimold, M., Smolka, M.N., Zimmer, A., Batra, A., Knobel, A., Solbach, C., Mundt, A., Smoltczyk, H.U., Goldman, D., Mann, K., Reischl, G., Machulla, H.J., Bares, R., Heinz, A., 2007. Reduced availability of serotonin transporters in obsessive–compulsive disorder correlates with symptom severity – a [^{11}C]DASB PET study. J. Neural. Transm. 114, 1603–1609.

Shapira, N.A., Liu, Y., He, A.G., Bradley, M.M., Lessig, M.C., James, G.A., Stein, D.J., Lang, P.J., Goodman, W.K., 2003. Brain activation by disgust-inducing pictures in obsessive–compulsive disorder. Biol. Psychiatry 54, 751–756.

Simpson, H.B., Lombardo, I., Slifstein, M., Huang, H.Y., Hwang, D.R., Abi-Dargham, A., Liebowitz, M.R., Laruelle, M., 2003. Serotonin transporters in obsessive–compulsive disorder: a positron emission tomography study with [^{11}C]McN 5652. Biol. Psychiatry 54, 1414–1421.

Stark, R., Schienle, A., Walter, B., Kirsch, P., Sammer, G., Ott, U., Blecker, C., Vaitl, D., 2003. Hemodynamic responses to fear and disgust-inducing pictures: an fMRI study. Int. J. Psychophysiol. 50, 225–234.

Stein, D.J., Arya, M., Pietrini, P., Rapoport, J.L., Swedo, S.E., 2006. Neurocircuitry of disgust and anxiety in obsessive–compulsive disorder: a positron emission tomography study. Metab. Brain Dis. 21, 267–277.

Stein, D.J., Liu, Y., Shapira, N.A., Goodman, W.K., 2001. The psychobiology of obsessive–compulsive disorder: how important is the role of disgust? Cur. Psychiatry Rep. 3, 281–287.

Stengler-Wenzke, K., Muller, U., Angermeyer, M.C., Sabri, O., Hesse, S., 2004. Reduced serotonin transporter-availability in obsessive–compulsive disorder (OCD). Eur. Arch. Psychiatry Clin. Neurosci. 254, 252–255.

van der Wee, N.J., Stevens, H., Hardeman, J.A., Mandl, R.C., Denys, D.A., van Megen, H.J., Kahn, R.S., Westenberg, H.M., 2004. Enhanced dopamine transporter density in psychotropic-naive patients with obsessive–compulsive disorder shown by [^{123}I]{beta}-CIT SPECT. Am. J. Psychiatry 161, 2201–2206.

Wilson, A.A., Garcia, A., Jin, L., Houle, S., 2000a. Radiotracer synthesis from [^{11}C]-iodomethane: a remarkably simple captive solvent method. Nucl. Med. Biol. 27, 529–532.

Wilson, A.A., Ginovart, N., Hussey, D., Meyer, J., Houle, S., 2002. In vitro and in vivo characterisation of [^{11}C]-DASB: a probe for in vivo measurements of the serotonin transporter by positron emission tomography. Nucl. Med. Biol. 29, 509–515.

Wilson, A.A., Ginovart, N., Schmidt, M., Meyer, J.H., Threlkeld, P.G., Houle, S., 2000b. Novel radiotracers for imaging the serotonin transporter by positron emission tomography: synthesis, radiosynthesis, and in vitro and ex vivo evaluation of ^{11}C-labeled 2-(phenylthio)araalkylamines. J. Med. Chem. 43, 3103–3110.

Zitterl, W., Aigner, M., Stompe, T., Zitterl-Eglseer, K., Gutierrez-Lobos, K., Schmidl-Mohl, B., Wenzel, T., Demal, U., Zettinig, G., Hornik, K., Thau, K., 2007. [^{123}I]-beta-CIT SPECT imaging shows reduced thalamus–hypothalamus serotonin transporter availability in 24 drug-free obsessive–compulsive checkers. Neuropsychopharmacology 32, 1661–1668.

Behavioral/Systems/Cognitive

Contribution of Dopamine D1 and D2 Receptors to Amygdala Activity in Human

Hidehiko Takahashi,[1,3] Harumasa Takano,[1] Fumitoshi Kodaka,[1] Ryosuke Arakawa,[1] Makiko Yamada,[1] Tatsui Otsuka,[1] Yoshiyuki Hirano,[2] Hideyuki Kikyo,[1] Yoshiro Okubo,[4] Motoichiro Kato,[5] Takayuki Obata,[2] Hiroshi Ito,[1] and Tetsuya Suhara[1]

Departments of [1]Molecular Neuroimaging and [2]Biophysics, Molecular Imaging Center, National Institute of Radiological Sciences, Chiba 263-8555 Japan, [3]Precursory Research for Embryonic Science and Technology, Japan Science and Technology Agency, Saitama, 332-0012, Japan, [4]Department of Neuropsychiatry, Nippon Medical School, Tokyo 113-8603, Japan, and [5]Department of Neuropsychiatry, Keio University School of Medicine, Tokyo 160-8582, Japan

Several animal studies have demonstrated functional roles of dopamine (DA) D1 and D2 receptors in amygdala activity. However, the contribution of DA D1 and D2 receptors to amygdala response induced by affective stimuli in human is unknown. To investigate the contribution of DA receptor subtypes to amygdala reactivity in human, we conducted a multimodal *in vivo* neuroimaging study in which DA D1 and D2 receptor bindings in the amygdala were measured with positron emission tomography (PET), and amygdala response induced by fearful faces was assessed by functional magnetic resonance imaging (fMRI) in healthy volunteers. We used multimodality voxelwise correlation analysis between fMRI signal and DA receptor binding measured by PET. DA D1 binding in the amygdala was positively correlated with amygdala signal change in response to fearful faces, but DA D2 binding in the amygdala was not related to amygdala signal change. DA D1 receptors might play a major role in enhancing amygdala response when sensory inputs are affective.

Introduction

The amygdala plays a central role in processing affective stimuli, and in particular, threatening stimuli in the brain (LeDoux, 2000). The amygdala receives a moderate innervation of dopaminergic fibers (Asan, 1998), and both dopamine (DA) D1 and D2 receptors are expressed in this region (Ito et al., 2008), although the latter exhibit lower expression (Scibilia et al., 1992). DA release in the amygdala is increased in response to stress (Inglis and Moghaddam, 1999). It has been shown in animal studies that DA potentiates the response of the amygdala by augmenting excitatory sensory input and attenuating inhibitory prefrontal input to the amygdala (Rosenkranz and Grace, 2002). Systemic and local applications into the amygdala of D1 agonist and antagonist are known to potentiate and decrease fear response in animals, respectively. Although some studies reported that applications of D2 agonist and antagonist induced similar effects, the results were less consistent compared with D1-mediated effects (for review, see Pezze and Feldon, 2004; de la Mora et al., 2009).

A human functional magnetic resonance imaging (fMRI) study reported that doparminergic drug therapy such as levodopa or DA agonists partially restored amygdala response due to emotional task in Parkinson's disease patients who showed no significant amygdala response during drug-off states (Tessitore et al., 2002). In addition, another fMRI study of healthy volunteers has demonstrated that amphetamine potentiated the response of the amygdala during an emotional task (Hariri et al., 2002). More recently, Kienast et al. (2008) reported that dopamine storage capacity in human amygdala, measured with 6-[^{18}F]fluoro-L-DOPA positron emission tomography (PET), was positively correlated with functional magnetic resonance imaging (fMRI) signal changes in amygdala. However, the contribution of DA D1 and D2 receptors to amygdala response induced by affective stimuli is unknown in human. To investigate the relation between amygdala reactivity and dopamine receptor subtype, we conducted a multimodal *in vivo* neuroimaging study in which DA D1 and D2 receptor bindings in the amygdala were measured with PET, and amygdala response by novel faces with either neutral or fearful expression was assessed with fMRI. Based on animal pharmacological studies, we hypothesized that D1, but not D2 receptors, would predict amygdala response.

Received Nov. 17, 2009; revised Jan. 8, 2010; accepted Jan. 8, 2010.

This study was supported by a consignment expense for Molecular Imaging Program on "Research Base for PET Diagnosis" from the Ministry of Education, Culture, Sports, Science and Technology. Takanori Kochiyama and Yoko Ikoma are greatly acknowledged for her comments. We thank K. Tanimoto and T. Shiraishi for their assistance in performing the PET experiments at the National Institute of Radiological Sciences. We also thank Y. Fukushima, K. Suzuki, and I. Izumida of the National Institute of Radiological Sciences for their help as clinical research coordinators.

Correspondence should be addressed to Hidehiko Takahashi, Department of Molecular Neuroimaging, National Institute of Radiological Sciences, 9-1, 4-chome, Anagawa, Inage-ku, Chiba, Chiba 263-8555, Japan. E-mail: hidehiko@nirs.go.jp.

DOI:10.1523/JNEUROSCI.5689-09.2010

 0270-6474/10/303043-05$15.00/0

Materials and Methods

Subjects

Twenty-one male volunteers [mean age 23.1 ± (SD) 3.6 years] were studied. They did not meet the criteria for any psychiatric disorder based on unstructured psychiatric screening interviews. None of the controls were taking alcohol at the time, nor did they have a history of psychiatric disorder, significant physical illness, head injury, neurological disorder, or alcohol or drug dependence. All subjects were right-handed according to the Edinburgh Handedness Inventory. All subjects underwent MRI to rule out cerebral anatomic abnormalities. After complete explanation of the study,

written informed consent was obtained from all subjects, and the study was approved by the Ethics and Radiation Safety Committee of the National Institute of Radiological Sciences, Chiba, Japan.

fMRI procedure

Stimulus materials were taken from the Karolinska Directed Emotional Faces (KDEF) (Lundqvist et al., 1998). Thirty neutral and 30 fear faces were used, with half of them being male faces. The pictures were projected via a computer and a telephoto lens onto a screen mounted on a head-coil. The experimental design consisted of 5 blocks for each of the 2 conditions (neutral, fear) interleaved with 21 s rest periods. The order of presentation for the 2 conditions (neutral and fear) was randomized. During the baseline condition, subjects viewed a crosshair pattern projected to the center of the screen. In each 21 s block, 6 different faces of the same emotional class were presented for 3.5 s each. During the scans, the subjects were instructed to judge the gender of each face using selection buttons.

fMRI scanning

The images were acquired with a 3.0 Tesla Excite system (General Electric). Functional images of 126 volumes were acquired with T2*-weighted gradient echo planar imaging sequences sensitive to the blood oxygenation level-dependent (BOLD) contrast. Each volume consisted of 40 transaxial contiguous slices with a slice thickness of 3 mm to cover almost the whole brain (flip angle, 90°; echo time, 50 ms; repetition time, 3500 ms; matrix, 64 × 64; field of view, 24 × 24 cm).

Analysis of fMRI data

Data analysis was performed with the statistical parametric mapping software package (SPM2) (Wellcome Department of Cognitive Neurology, London, UK) running with MATLAB (MathWorks). All volumes were realigned to the first volume of each session to correct for subject motion and were spatially normalized to the standard space defined by the Montreal Neurological Institute (MNI) template. After normalization, all scans had a resolution of $2 \times 2 \times 2$ mm^3. Functional images were spatially smoothed with a three-dimensional isotropic Gaussian kernel (full-width at half-maximum of 8 mm). Low-frequency noise was removed by applying a high-pass filter (cutoff period = 128 s) to the fMRI time series at each voxel. A temporal smoothing function was applied to the fMRI time series to enhance the temporal signal-to-noise ratio. Significant hemodynamic changes for each condition were examined using the general linear model with boxcar functions convolved with a hemodynamic response function. Statistical parametric maps for each contrast of *t*-statistic were calculated on a voxel-by-voxel basis.

We assessed the contrasts of fear and neutral minus baseline (F&N-B). A random effects model, which estimates the error variance for each condition across the subjects, was implemented for group analysis. The contrast images were obtained from single-subject analysis and entered into the group analysis. A one-sample *t* test was applied to determine group response for each effect. Significant amygdala activations were identified if they reached the extent threshold of $p < 0.05$ corrected for multiple comparisons, with a height threshold of $p < 0.001$, uncorrected.

PET scanning

After the fMRI session, each participant underwent PET scanning. The interval between fMRI session and PET scan was 3–5 h. PET studies were performed on ECAT EXACT HR+ (CTI-Siemens). The system provides 63 planes and a 15.5 cm field of view. To minimize head movement, a head fixation device (Fixster) was used. A transmission scan for attenuation correction was performed using a germanium 68–gallium 68 source. Acquisitions were done in three-dimensional mode with the interplane septa retracted. For evaluation of D1 receptors, a bolus of 219.7 ± 6.9 MBq of [^{11}C]SCH23390 with specific radioactivities (95.7 ± 35.5 GBq/μmol) was injected intravenously from the antecubital vein with a 20 ml saline flush. For evaluation of extrastriatal DA D2 receptors, a bolus of 218.1 ± 14.7 MBq of [^{11}C]FLB457 with high specific radioactivities (221.6 ± 94.9 GBq/μmol) was injected in the same way. Dynamic scans were performed for 60 min for [^{11}C]SCH23390 and 90 min for [^{11}C]FLB457 immediately after the injection. All emission scans were reconstructed with a Hanning filter cutoff frequency of 0.4 (full-width at half-maximum, 7.5 mm). MRI was performed on Gyroscan NT (Philips Medical Systems) (1.5 T). T1-weighted images of the brain were obtained for all subjects. Scan parameters were 1-mm-thick, three-dimensional T1 images with a transverse plane (repetition time/echo time, 19/10 ms; flip angle, 30°; scan matrix, 256 × 256 pixels; field of view, 256 × 256 mm; and number of excitations, 1).

Quantification of DA D1 and D2 receptors

Quantitative analysis was performed using the three-parameter simplified reference tissue model (Lammertsma and Hume, 1996; Olsson et al., 1999). The cerebellum was used as a reference region because it has been shown to be almost devoid of DA D1 and D2 receptors (Farde et al., 1987; Olsson et al., 1999; Suhara et al., 1999). The model provides an estimation of the binding potential ($BP_{ND\ (nondisplaceable)}$) (Innis et al., 2007), which is defined by the following equation: $BP_{ND} = k_3/k_4 = f_2 B_{max}/\{K_d [1 + \Sigma_i F_i/K_{di}]\}$, where k_3 and k_4 describe the bidirectional exchange of tracer between the free compartment and the compartment representing specific binding, f_2 is the "free fraction" of nonspecifically bound radioligand in brain, B_{max} is the receptor density, K_d is the equilibrium dissociation constant for the radioligand, and F_i and K_{di} are the free concentration and dissociation constant of competing ligands, respectively (Lammertsma and Hume, 1996). Tissue concentrations of the radioactivities of [^{11}C]SCH23390 and [^{11}C]FLB457 were obtained from regions of interest (ROIs) defined on PET images of summated activity for 60 min and 90 min, respectively, with reference to the individual MRIs coregistered on summated PET images and the brain atlas. Given our hypothesis of amygdala activation during viewing novel neutral and fearful faces, ROIs were set on the bilateral amygdala. The method for defining the boundaries of the amygdala was adapted from previously described methods (Kates et al., 1997; Convit et al., 1999). In short, the amygdala ROIs consisted of three axial slices. The anterior and posterior boundaries were identified at the level of the optic chiasm and the temporal horn of the lateral ventricle, respectively. The superior and inferior-lateral boundaries were identified at the level of the mammalian body and the temporal lobe white matter and extension of the temporal horn, respectively. We also created parametric images of BP_{ND} using the basis function method (Gunn et al., 1997) to conduct voxelwise SPM analysis in addition to ROI analysis.

Statistical analysis

ROI correlation analysis. Estimates of percentage signal change of fear vs baseline condition were extracted from the amygdala for each participant using the MarsBaR toolbox (Brett et al., 2002). The bilateral amygdala ROIs were defined from the WFU-Pickatlas SPM tool (Maldjian et al., 2003) with the aal atlas (Tzourio-Mazoyer et al., 2002). Correlation between BP_{ND} of [^{11}C]SCH23390 and [^{11}C]FLB457 in the bilateral amygdala and bilateral amygdala fMRI signal change were calculated using SPSS.

Confirmatory SPM correlation analysis. Parametric images of BP_{ND} of [^{11}C]SCH23390 and [^{11}C]FLB457 were analyzed using SPM2. Exactly the same image preprocessings of normalization and smoothing that were used in fMRI data analysis were applied to parametric images of BP_{ND}. To conduct multimodality voxelwise correlation analysis between the BOLD signal and DA receptor binding, we used the biological parametric mapping toolbox for SPM (Casanova et al., 2007). Significant clusters were identified if they reached the extent threshold of $p < 0.05$ corrected for multiple comparisons, with a height threshold of $R > 0.6$ ($p < 0.003$ uncorrected).

Results

Since the face pictures consisted of Caucasian faces (racial outgroup), even novel neutral faces produced amygdala response in several participants (Hart et al., 2000; Schwartz et al., 2003), leading to a blunted contrast of fear minus neutral. Therefore, we combined neutral and fear conditions and used F&N-B contrast for analyses. Group analysis of F&N-B contrast revealed significant bilateral amygdala responses [right amygdala (26, 0, −26), $t = 4.43$, 93 voxels, left amygdala (−20, −2, −26), $Z = 4.96$, 101

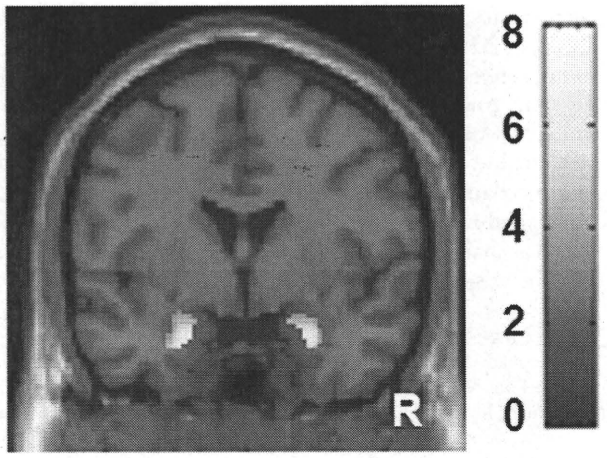

Figure 1. Images showing brain response induced by fear and neutral minus baseline condition. Bilateral amygdala responses are shown. The bar shows the range of the *t*-value. R indicates right.

voxels] (Fig. 1). The mean BP_{ND} of [^{11}C]SCH23390 in the right and left amygdala were 0.38 ± 0.08 and 0.39 ± 0.11, respectively. The mean BP_{ND} of [^{11}C]FLB457 in the right and left amygdala were 2.49 ± 0.50 and 2.50 ± 0.44, respectively.

Correlation analysis of biological parametric mapping revealed that the BP_{ND} value of [^{11}C]SCH23390 in the right amygdala was positively correlated with the BOLD signals in the right amygdala of F&N-B contrast [peak (28, 2, −28), 24 voxels] (Fig. 2A). ROIs analysis also revealed a similar significant correlation ($r = 0.59$, $p = 0.005$) in the right amygdala (Fig. 2B), but not in the left amygdala ($r = 0.18$, $p = 0.43$). According to biological parametric mapping analysis, the BP_{ND} value of [^{11}C]FLB457 in the amygdala was not correlated with BOLD signals in the amygdala of F&N-B contrast. ROIs analysis showed that right and left amygdala D2 binding was not correlated with the BOLD signals in the right ($r = 0.26$, $p = 0.27$) and left amygdala ($r = 0.28$, $p = 0.23$), respectively. Both biological parametric mapping analysis and ROIs analysis showed that D1 binding in the right and left amygdala was not correlated with D2 binding in the right ($r = 0.24$, $p = 0.30$) and left amygdala ($r = 0.16$, $p = 0.49$), respectively. We used anatomically defined ROIs of the amygdala rather than functional ROIs defined by fMRI in the ROI correlation analysis because it is difficult to place functionally defined ROIs on individual PET data. Anatomically defined ROIs of the amygdala were larger than functionally defined amygdala ROIs. This fact was advantageous in increasing the signal-to-noise ratio in the PET analysis, but led to blunted BOLD signal changes in the amygdala. However, BOLD signal changes derived from both ROI methods were highly correlated with each other. For example, very high correlation ($r = 0.80$, $p < 0.001$) was observed in the right amygdala. Thus, regardless of ROI definition method, we obtained similar results from ROI correlation analyses between BOLD signal changes and DA receptor binding in the amygdala.

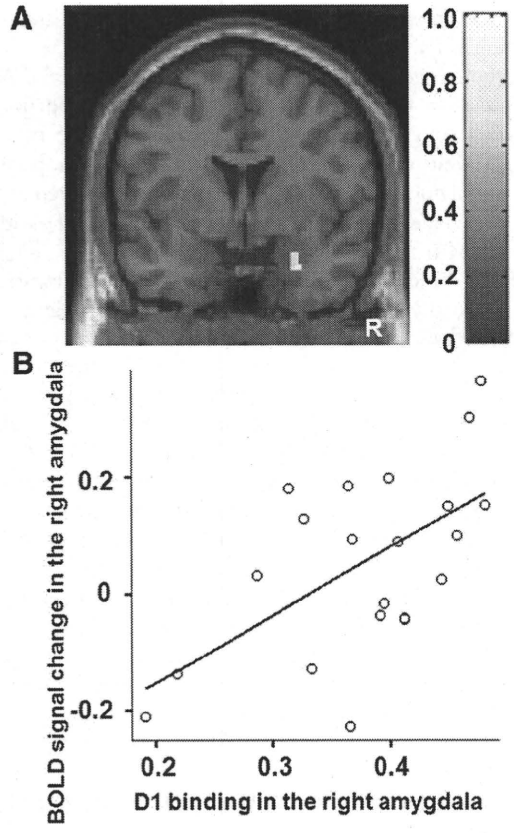

Figure 2. ***A***, SPM correlation analysis revealed significant positive linear correlations between D1 binding in the right amygdala and right amygdala signal change. The bar shows the range of the correlation coefficient. ***B***, ROI correlation analysis also revealed similar correlations. R indicates right.

Discussion

Using a multimodality *in vivo* neuroimaging approach, we first directly compared amygdala DA D1 and D2 receptor bindings, indices of receptor availability, with amygdala response evoked by novel or fearful stimuli in human. We found that DA D1 receptors, but not D2 receptors, predicted amygdala response induced by novel facial stimuli with either neutral or fearful expression. Our findings broaden our knowledge about dopaminergic transmission in amygdala response beyond the recent study (Kienast et al., 2008) that elucidated the relation between presynaptic dopamine synthesis and amygdala reactivity.

Human neuroimaging studies reported that DA potentiated amygdala response evoked by affective stimuli (Hariri et al., 2002; Tessitore et al., 2002). In rat studies, Rosenkranz and Grace (2002) demonstrated that DA enhances the response of the amygdala by augmenting excitatory sensory input via DA D2 receptor stimulation and attenuating inhibitory prefrontal input to the amygdala through DA D1 receptor stimulation. More recently, it was demonstrated that both D1 and D2 receptor stimulations directly enhanced the excitability of amygdala projection neurons via postsynaptic mechanism (Rosenkranz and Grace, 2002; Kröner et al., 2005; Yamamoto et al., 2007). Amygdala projection neurons are under inhibitory control by GABAergic interneurons (Royer et al., 1999). Both projection neurons and interneurons in the amygdala express DA D1 and D2 receptors (Rosenkranz and Grace, 1999). It has been shown that DA and D1 receptor stimulation augments interneuron excitability and increases the frequency of IPSC in amygdala projection neurons (Kröner et al., 2005). This is a counterintuitive result, considering the fact that DA disinhibits amygdala response *in vivo*. However, Marowsky et al. (2005) found that a subpopulation of amygdala interneurons (paracapsular intercalated cells), located between the major input and output stations of amygdala, is suppressed by DA through D1 receptor stimulation. DA D2 receptors also play a role in disinhibiting amygdala response by decreasing inhibi-